ROYAL INSTITUTE
OF TECHNOLOGY

Phase fluctuation phenomena in superconductors

ANDREAS ANDERSSON

Doctoral thesis

Department of Theoretical Physics
KTH Royal Institute of Technology
Stockholm, Sweden 2012

TRITA-FYS 2012:28
ISSN 0280-316X
ISRN KTH/FYS/–12:28–SE
ISBN 978-91-7501-380-0

KTH Teoretisk fysik
AlbaNova Universitetscentrum
SE-106 91 Stockholm, SWEDEN

Akademisk avhandling som med tillstånd av Kungl Tekniska högskolan framlägges till offentlig granskning för avläggande av teknologie doktorsexamen i teoretisk fysik torsdagen den 14:e juni 2012 kl. 10:00 i sal FB42, AlbaNova Universitetscentrum, KTH, Stockholm.

© Andreas Andersson, 2012

Tryck: Universitetsservice, US-AB

Typsatt med LaTeX

Abstract

Superconductivity results from Cooper-paired electrons forming a macroscopic quantum state. In superconductors of low dimensionality, as well as in systems with low superfluid density, fluctuations in the phase of the wavefunction describing this quantum state are enhanced. These phase fluctuations can significantly alter transport properties and may, more dramatically, also lead to the destruction of the superconducting state. This thesis presents results from theoretical modeling and large-scale computer simulations of effects due to superconducting phase fluctuations in variety of one- and two-dimensional superconducting systems of experimental and theoretical interest.

The Nernst effect, thermal conductivity, and electrical resistivity in granular thin-film superconductors and Josephson junctions are investigated, using a phase-only model with either relaxational Langevin, or resistively and capacitively shunted Josephson junction (RCSJ) dynamics. A heat current expression for these dynamics is explicitly derived. The transport coefficients are calculated as functions of temperature, magnetic field, and disorder. In strong magnetic fields, transport is severely affected by geometric frustration effects.

In two-dimensional superconducting systems, the Berezinskii-Kosterlitz-Thouless transition separates the superconducting and normal phases. By a combination of renormalization group techniques and simulations, the scaling properties of the resistivity and current-voltage characteristics at this special phase transition are investigated. For zero magnetic fields, the analysis reveals a strong multiplicative logarithmic correction to the scaling of the resistivity. By instead approaching the transition in an asymptotically vanishing field, the correction can be avoided. This should be of relevance for the interpretation of both experiments and simulation data.

Sudden jumps of 2π in the phase of the superconducting order parameter of thin superconducting wires, induced by quantum fluctuations, so called quantum phase slips (QPS), cause dissipation and are believed to destroy superconductivity in thin enough wires, even at zero temperature. Recent experimental evidence supports this claim. Here, quantum phase slips are studied by means of grand canonical Monte Carlo simulations, based on a reformulation of a microscopically derived action for the QPS. A method of obtaining the probability amplitude for QPS, and also the response of the system to an applied charge displacement, is formulated and employed in the simulations.

Preface

This thesis is a result of my time as a PhD student at the Department of Theoretical Physics, KTH Royal Institute of Technology, during the years 2007 – 2012. The thesis is divided into two parts. The first part is intended as an introduction to the topics of the appended papers. The second part contains the papers listed below.

Appended papers

Paper 1. Anomalous Nernst effect and heat transport by vortex vacancies in granular superconductors, Andreas Andersson and Jack Lidmar, *Physical Review B* 81, 060508(R) (2010) [1].

Paper 2. Influence of vortices and phase fluctuations on thermoelectric transport properties of superconductors in a magnetic field, Andreas Andersson and Jack Lidmar, *Physical Review B* 83, 174502, (2011) [2].

Paper 3. Scaling, finite size effects, and crossovers of the resistivity and current-voltage characteristics in two-dimensional superconductors , Andreas Andersson and Jack Lidmar, *Preprint, arXiv:1203.5317*, (2012) [3].

Paper 4. Modeling and simulations of quantum phase slips in ultrathin superconducting wires, Andreas Andersson and Jack Lidmar, *Manuscript*, (2012) [4].

My contributions to the papers

Paper 1. I wrote all simulation code, carried out the simulations, analyzed the data, produced the figures, and co-wrote the paper.

Paper 2. I did parts of the analytical calculations, wrote all simulation, carried out the simulations, analyzed the data, produced the figures, and co-wrote the paper.

Paper 3. I found the apparent inconsistency in the scaling properties of the resistivity that motivated this paper. The scaling analysis was done together with Jack Lidmar. I wrote all simulation code, performed the simulations and data analysis, produced the figures, and wrote the first draft of the paper.

Paper 4. I wrote all simulation code, performed the simulations and the data analysis. The writing of the paper was a joint effort.

Acknowledgements

"No man is an island." This is generally true in science and in most branches of life. I'm certainly no exception, as I'm indebted to many people who have helped me make this thesis a reality.

First I would like to deeply thank my supervisor Jack Lidmar, who has always been there to answer any question of mine. Your guidance, expertise and kind ways have been truly invaluable. A warm gratitude also to Mats Wallin for letting me join the Theoretical Physics department as a PhD student.

Thanks to the entire department staff for providing a nice working atmosphere during my over five years here. My previous roommates, Marios Nikolaou, Martin Lindén and Anders Biltmo, are especially remembered. My present roomies, Hannes Meier, Oskar Palm and Johan Carlström are likewise acknowledged. You make our room a great place for research, and constantly fill it with heated discussions and laughter. Hannes, my good old friend, keep this spirit alive also without me! I've also very much enjoyed the company of Egor Babaev, Richard Tjörnhammar and Erik Brandt during many coffee and lunch breaks. Erik, your comradery during our almost ten years together at KTH has been fabulous.

My large family, the Anderssons, the Archentis, the Ernevings and the Bratels, deserve a large part of the credit for their care, support, and persistent curiosity in understanding what it is that I do in my research. Mum and dad, I guess the home experimental kits you bought me as a child finally paid off, huh?

Lastly and above all, I thank Yaël, my true love, for making my life a wonderful one to live.

Andreas Andersson,
Stockholm, May 13, 2012.

Contents

Part I

Background

Chapter 1

Introduction: Superconductivity

The spring of 2012 marks the 101st birthday of the field of superconductivity. Despite its considerable age, the birthday child is still very much alive and kicking, although some might say it was reborn only 26 years ago.

The original discovery was made April 8th 1911 by the Dutch physicist Heike Kamerlingh Onnes, who noticed how the electrical resistance in mercury suddenly vanished as the metal was cooled below 4.15 K [5] ($\sim$ -269 °C). Ironically (and amazingly), in the very same day he also witnessed the superfluid transition of liquid helium-4, which was used as refrigerant in the experiment, but without realizing it! [6] In fact, superconductors and superfluids are closely akin to each other. The most spectacular property of a superconductor is zero electrical resistance. In optimal conditions, a current induced in a superconducting ring can have an estimated lifetime vastly exceeding the age of our universe [7]. A superfluid, on the other hand, shows no flow resistance, i.e., it has zero viscosity and flows frictionless past any surface. The underlying physical mechanism is the same in both cases, namely Bose-Einstein condensation – a quantum mechanical phenomena in which a macroscopic number of particles condense into the lowest energy quantum state. The difference lies mainly in that superfluids consist of condensed electrically neutral bosons, while the particles responsible for superconductivity are charged, made up of two electrons with opposite spin and momenta, bound together by a phonon-mediated interaction. These so called *Cooper pairs* are, in contrast to single electrons, bosonic in nature, enabling them to Bose-Einstein condense into a charged superfluid. A full microscopic understanding of the Cooper pairing phenomena was reached in 1957 with the celebrated paper by Bardeen, Cooper and Schrieffer (BCS) [8]. Almost 30 years later, confusion and great excitement followed in the wake of the milestone discovery of superconductivity in ceramic copper-oxide materials, so called *cuprates* in 1986 [9], as the BCS theory could not explain how this was possible. Since then, much progress has been made in developing new materials, leading to critical temperatures of well over 100 K ($\sim$ -173 °C) in many high-T_c superconductors. On the theory side, however, the problem of understanding the microscopic mechanism behind high-T_c superconductivity remains unsolved to this very day.

The field of superconductivity has long been, and still continues to be, a major driving force in physics. Leaving the high-T_c problem aside, superconductivity has proven extremely fruitful in producing new physical theories and concepts, and useful technology. Today superconductors can be found in many hospitals, where large superconducting coils produce the massive magnetic flux strengths needed in *nuclear magnetic resonance imaging* (NMRI) machines. Superconducting electromagnets are also used in particle accelerators (e.g. LHC), experimental fusion reactors, and in magnetic levitation trains. Other large-scale applications include electrical *energy storage* and extreme high current *power transmission* in high-T_c superconductor cables cooled by liquid nitrogen. The first commercial project of this kind saw light already 2008 in the U.S. [10] and a second one is planned in Germany [11]. A particularly promising use of superconductors is in nanoelectronics. Extremely sensitive magnetometers, so called *SQUID*s, are already well established, and many other interesting electronic detectors and devices providing a plethora of applications, exist or are in development. Furthermore, circuits based on superconducting *Josephson junctions* are today considered as probable candidates for the elementary building blocks, *qubits*, of a future quantum computer [12, 13]. However, for further technological advances in this field, an even better understanding of fundamental physical phenomena in superconductors, especially those of reduced dimensionality, will certainly be key.

The research of the present thesis is in this exploratory spirit. It concerns fundamental aspects, such as electric and thermal transport, and critical scaling properties, in one- and two-dimensional superconducting systems, which are both of theoretical and experimental interest. Our approach is based on a combination of theoretical modeling and large-scale computer simulations. We formulate simplistic models, but with enough detail to capture the essential physics we wish to investigate. Usually, though, these models are sufficiently complicated to render exact analytical solutions of them impossible, other than in special limits. Here the main tool of our analysis, computer simulations, is invaluable, since it enables exact solutions (up to numerical and statistical errors) of these models. The purpose of this research is two-fold: To explore the theoretical models and provide a deeper understanding of their physical relevance. More importantly, through our work we also wish to guide experimentalists in their research, and ultimately suggest new exciting phenomena to look for in these systems.

This first chapter introduces the immensely successful phenomenological Ginzburg-Landau theory and related concepts, along with a discussion of vortices – an important and reoccurring entity in this thesis. This lays the foundation for the other chapters. Chapter 2 reviews phenomena and models connected to superconducting phase fluctuations, the main topic of our research. Chapter 3 discusses the renormalization group idea, which is then naturally connected to the concept of scaling, both at classical and quantum phase transitions. This provides a background to Paper 3 and 4. In Chapter 4 Monte Carlo simulations, as well as some general numerical methods of solving stochastic differential equations are introduced. In addition, the main technical aspects of the models employed in our research are discussed in some detail. The concluding chapter is intended as a more specific summary of the results of the appended papers.

1.1 Ginzburg-Landau theory

The Ginzburg-Landau (GL) theory is an extension of Landau's general theory of second order phase transitions, introducing the concept of an *order parameter* which is nonzero in the ordered phase and zero in the disordered phase. In GL theory [14] the order parameter is a complex wavefunction describing the condensed Cooper pairs in a superconductor

$$\Psi(\boldsymbol{r}) = |\Psi(\boldsymbol{r})|e^{i\theta(\boldsymbol{r})} = \sqrt{n_s(\boldsymbol{r})}e^{i\theta(\boldsymbol{r})}, \tag{1.1}$$

where $n_s(\boldsymbol{r}) = |\Psi(\boldsymbol{r})|^2$ is the local Cooper pair number density. Assuming that Ψ is small close to the transition temperature and changes slowly in space, the total free energy of the superconductor can be expressed as an expansion in the order parameter and its gradients. From general symmetry considerations [15] one can show that the expansion must only include terms of even powers. The result is the *GL free energy functional*

$$F = F_n + \int \mathrm{d}^d r \left[\alpha |\Psi(\boldsymbol{r})|^2 + \frac{\beta}{2}|\Psi(\boldsymbol{r})|^4 + \frac{1}{2m^*}|(-i\hbar\nabla - q\boldsymbol{A})\Psi(\boldsymbol{r})|^2 + \frac{\boldsymbol{B}^2}{2\mu_0}\right], \tag{1.2}$$

where $\boldsymbol{B} = \nabla \times \boldsymbol{A}$ is the magnetic flux density and F_n the free energy of the normal state. Landau's theory of phase transitions tells us that the coefficient $\alpha(T)$ to lowest order around the mean field transition temperature T_c^0 has the form $\alpha(T) = \alpha_0(T - T_c^0)$, with $\alpha_0 > 0$, so that it is positive above the critical temperature, and changes sign at the phase transition. The mean field solution (taking Ψ to be spatially constant) that minimizes the GL free energy is thus

$$\Psi_0 = \begin{cases} \sqrt{-\alpha/\beta}, & T < T_c^0, \\ 0, & T \geq T_c^0. \end{cases} \tag{1.3}$$

When including the effects of fluctuations, the true transition takes place at a temperature below the mean field transition temperature T_c^0. The effects are particularly dramatic in one and two dimensions. More about this in Chapter 2.

Furthermore, we must have $\beta > 0$, since would β be negative, the free energy could be made arbitrarily small (negative and large) by making Ψ large, a situation for which the free energy expansion above is obviously not applicable. Note also that the coefficient in front of the gradient term is generally positive in Landau theory. Here it can be fixed by remembering that in quantum mechanics the gauge-invariant form of mass times velocity for a particle of charge q and mass m^* is

$$m^*\boldsymbol{v} = -i\hbar\nabla - q\boldsymbol{A}. \tag{1.4}$$

From this we see that the gradient term in (1.2) is nothing but the kinetic energy density $n_s m^* \boldsymbol{v}^2/2$ if the coefficient is set to $1/2m^*$.

By minimizing the GL free energy (1.2), with respect to variations in Ψ we get the *first GL equation*

$$\alpha\Psi + \beta|\Psi|^2\Psi + \frac{1}{2m^*}(-i\hbar\nabla - q\boldsymbol{A})^2\Psi = 0 \tag{1.5}$$

Doing the same with respect to variations in the vector potential $\boldsymbol{A}$ together with Ampère's law, $\mu_0\boldsymbol{J} = \nabla \times \boldsymbol{B}$, relating the current density $\boldsymbol{J}$ to the curl of the magnetic field $\boldsymbol{B}$, yields *the second GL equation*

$$\boldsymbol{J} = \frac{q}{2m^*}(\Psi^*(-i\hbar\nabla - q\boldsymbol{A})\Psi + \Psi(i\hbar\nabla - q\boldsymbol{A})\Psi^*), \tag{1.6}$$

or equivalently, by rewriting Ψ in a polar form, given by (1.1), we have a *supercurrent*

$$\boldsymbol{J} = \frac{q}{m^*}|\Psi(\boldsymbol{r})|^2(\hbar\nabla\theta(\boldsymbol{r}) - q\boldsymbol{A}). \tag{1.7}$$

The expression for the supercurrent above is exactly that found from quantum mechanics for particles with effective charge q and mass m^* in presence of a magnetic field $\boldsymbol{B} = \nabla \times \boldsymbol{A}$ (this is yet another way of fixing the gradient coefficient). At the time of birth of the GL theory (1950), the phenomenon of Cooper pairing was not known, and therefore Landau and Ginzburg identified q with the charge of an electron $-e$. The correct form of the GL free energy with $q = -2e$ (and $m^* = 2m$, two times the electron mass) was established by Gor'kov in 1959 [16] as he showed that the GL theory can be derived from the microscopic BCS theory. From here on we adopt this notation.

Now look at the first GL equation (1.5) above. Since each term in that expression must be of the same dimensionality, we know for example that $\alpha\Psi$ and $\frac{\hbar^2}{4m}\nabla^2\Psi$ (the gradient part of the kinetic term) have the same dimension. This implies the existence of a characteristic length ξ, relating the coefficients of the two terms so that $\frac{\hbar^2}{4m} = |\alpha|\xi^2$ (where $\alpha = -|\alpha|$ below T_c). This quantity is the *correlation length* (or *coherence length*) and can be written as

$$\xi = \sqrt{\frac{\hbar^2}{4m|\alpha|}}. \tag{1.8}$$

The coherence length sets the length scale of the fluctuations of the order parameter field Ψ in the model. Note that at $T = T_c$ the coefficient α goes to zero and ξ diverges, a general property of second order phase transitions.

The length scale on which fluctuations of the magnetic field $\boldsymbol{B}$ occur in the GL theory is set by the so called *penetration length* (or penetration depth) λ. This length can be derived by a similar dimensionality analysis as above. Combining the second GL equation (1.7) with Ampère's law we have

$$\nabla \times \boldsymbol{B} = \nabla \times \nabla \times \boldsymbol{A} = \mu_0\boldsymbol{J} = \frac{-2e\mu_0}{m}|\Psi(\boldsymbol{r})|^2(\hbar\nabla\theta(\boldsymbol{r}) + 2e\boldsymbol{A}), \tag{1.9}$$

which tells us that $\nabla \times \nabla \times \boldsymbol{A}$ has the same dimension as $(\mu_0(2e)^2|\Psi|^2/2m)\boldsymbol{A}$, so there is a length λ such that $\mu_0(2e)^2|\Psi|^2/2m = 1/\lambda^2$, giving the expression for the penetration depth

$$\lambda = \sqrt{\frac{2m}{\mu_0(2e)^2|\Psi|^2}}. \tag{1.10}$$

The ratio of these two length scales defines the dimensionless Ginzburg-Landau parameter $\kappa = \lambda/\xi$, the only free parameter needed to characterize a superconductor within the GL theory.

In an externally applied magnetic field $\boldsymbol{H}$, a superconductor will expel the field so that $\boldsymbol{B} = 0$ inside the material. This is the well-known *Meissner effect* [17]. More precisely, the $\boldsymbol{B}$ field is exponentially suppressed in a thin boundary layer of the order of the penetration depth λ. This is due to screening supercurrents setting up a field that cancels the applied field exactly. This can be easily verified by taking the curl of Eq. (1.9) and solving the resulting differential equation. Increasing the applied magnetic field, there are two distinctly different scenarios depending on the value of the GL parameter κ. Materials with small κ, a category in which most ordinary pure metals fall, lose their superconducting abilities at a certain critical field strength $H = H_c$, when the field starts penetrating the entire sample. These are called *type I* superconductors. The phase transition is of first order, i.e., there is some latent heat connected to it. *Type II* materials are those with a large κ, such as special metals, metal alloys and all high-T_c superconductors of various types. The difference between the two types lies in the sign of the surface energy of a normal-superconducting interface, parameterized by κ, which has profound consequences on the nature of the phase transition in a magnetic field. Ginzburg and Landau showed numerically in their original 1950 paper [14] that the sign change happens at exactly $\kappa = 1/\sqrt{2}$. In type II materials the surface energy is negative, and it can thus be energetically favorable to have a mix of normal and superconducting phases, since the free energy cost of a normal region could be compensated by the negative free energy contribution from the normal-superconducting interface. This is the so called *mixed phase*, or *Shubnikov phase* [18], after its experimental discoverer. It is present in an interval $H_{c1} < H < H_{c2}$ between the Meissner ($H < H_{c1}$) and the normal phase ($H > H_{c2}$).

1.2 Vortices

The normal regions where the applied magnetic field penetrates a type II superconductor in the mixed phase are called *vortex lines* or *vortices*. The flux carried by a vortex is quantized [19]. This fascinating property follows directly from taking a closed contour integral around the vortex line inside the superconductor, where the screening supercurrent given by Eq. (1.7) is zero

$$\oint \frac{\hbar}{2e}\nabla\theta(\boldsymbol{r}) \cdot d\boldsymbol{r} = \oint \boldsymbol{A} \cdot d\boldsymbol{r}. \tag{1.11}$$

The circulation of the vector potential is nothing but the flux Φ through the surface spanning the contour, i.e., the flux carried by the vortex

$$\oint \boldsymbol{A} \cdot d\boldsymbol{r} = \int \nabla \times \boldsymbol{A} \cdot d\boldsymbol{S} = \int \boldsymbol{B} \cdot d\boldsymbol{S} = \Phi. \tag{1.12}$$

The integral over the gradient of the phase field, on the other hand, must be a multiple of 2π for the complex order parameter field to be single valued, leading to the quantization condition

$$\Phi = \oint \frac{\hbar}{2e} \nabla\theta(\boldsymbol{r}) \cdot d\boldsymbol{r} = \frac{\hbar}{2e} 2\pi n = n\Phi_0, \quad n = 0, \pm 1, \pm 2, ..., \tag{1.13}$$

where $\Phi_0 = h/2e$ defines the *flux quantum*. In practice a vortex carrying more than one flux quantum Φ_0 is unstable and will decay into separate vortices with flux Φ_0 to maximize the normal-superconducting interface area, in order to minimize the total free energy.

Vortex phases

Interestingly, Ginzburg and Landau did not investigate the case $\kappa > 1/\sqrt{2}$, since they concluded from the negative surface energy that the superconducting state would be unstable there. When Abrikosov in 1953 showed that a mixed state was possible, with vortices forming a regular lattice, Landau disagreed and stopped the publication of this result [20]. Eventually the paper was published in 1957 [21]. However, by a numerical mistake, Abrikosov erroneously concluded that a square array was the energetically preferred one. This was rectified a couple of years later by Kleiner *et al.* [22], who showed that a triangular vortex lattice has a slightly lower energy. In Abrikosov's defense it must be said that the difference is very small, and so the crystalline structure in real materials can sometimes make a square solution favorable. In a mean field description the phase transition from the mixed phase to the normal phase is continuous, and happens roughly at a magnetic field when the vortices become so densely packed that the vortex lattice constant $a \approx (\Phi_0/B)^{1/2}$ is of the same order as the correlation length ξ, so that the vortex cores start to overlap.

In conventional low-T_c superconductors this mean field description is essentially correct, but in the case of high-T_c superconductors the increased effect of thermal fluctuations might induce a first order melting transition of the vortex lattice into a *vortex liquid* phase, which can occupy large portions of the phase diagram. The transition from the vortex liquid to the normal phase is merely a crossover around the upper critical field H_{c2}. In most real materials there are also different types of crystal defects that tend to disorder the vortex lattice and transform it into various *vortex glass* phases, depending on the density of defects (see [23, 24] for more details).

1.3 Vortex motion

Dissipation manifested as nonzero electrical resistivity in the mixed phase can on a phenomenological level be understood by considering moving vortices subjected to a viscous drag force [25]. When applying an external current density $\boldsymbol{J}$ to a perfectly clean superconductor, the vortex system will start to move due to a Lorentz force per unit length

$$\boldsymbol{F}_L = \boldsymbol{J} \times \boldsymbol{B}. \tag{1.14}$$

On a single vortex, the force per length is $\boldsymbol{F}_L = \boldsymbol{J} \times \boldsymbol{\Phi_0}$. If the vortex lattice has not yet melted, the entire lattice can move rigidly. A friction force $\boldsymbol{F}_f = -\eta \boldsymbol{v}$ will restrict the motion, so that the vortex velocity in steady state (where the two forces balance each other, $\boldsymbol{F}_L + \boldsymbol{F}_f = 0$) becomes $\boldsymbol{v} = \boldsymbol{J} \times \boldsymbol{B}/\eta$. The flow of the magnetic flux carried by the vortices produce an electric field $\boldsymbol{E} = -\boldsymbol{v} \times \boldsymbol{B}$, perpendicular to their motion and parallel to the current density $\boldsymbol{J}$ [26]. This results in a power dissipation $\boldsymbol{E} \cdot \boldsymbol{J}$ per unit volume, which can be detected as a nonzero electrical resistivity

$$\rho = B^2/\eta, \tag{1.15}$$

assuming $\boldsymbol{J} \perp \boldsymbol{B}$. True superconductivity with dissipationless flow of current is thus lost under the application of a current density $\boldsymbol{J} \perp \boldsymbol{B}$ in the mixed phase. However, motion of vortices can be prevented by balancing the Lorentz force with a pinning force $\boldsymbol{F}_p$ that is nonzero for $\boldsymbol{v} = 0$. In real superconductors such a force is always present due to disorder in the material. Furthermore, by introducing artificially created defects into the superconductor, the pinning force $\boldsymbol{F}_p$ can often be optimized to further increase the depinning current density $J_{\text{dep}} = F_p/B$, below which there is no vortex motion and hence no dissipation. Even so, in principle, in a finite pinning potential landscape of typical height U_0, vortices can still move due to thermal activation. A small but finite applied current density $\boldsymbol{J} \perp \boldsymbol{B}$ leads to a bias in the forward and backward hopping rates and thus to a directed vortex motion and a resistivity

$$\rho \sim e^{-U_0/k_B T}. \tag{1.16}$$

This process is usually referred to as *vortex creep* [27]. We finally note that, in the vortex glass phases it has been shown that the typical height of the barriers diverges so that $\rho \to 0$ as $J \to 0$ [28, 29], i.e., superconductivity is again recovered, at least in the linear response limit.

1.4 Thermoelectric effects and vortices

Vortices play an important role in the current-voltage characteristics of type II superconductors in the mixed state, as discussed in the previous section. Since vortices are also associated with some finite entropy and thus can carry heat, thermal transport or

phenomena where thermal and electric effects combine, the thermoelectric or thermomagnetic effects, can be strongly affected by vortex dynamics. The thermoelectric effects come in a number of different variants depending on the exact experimental setup, and are all named after one, or possibly, two 19th century physicists, e.g., Seebeck, Hall, Thomson, Peltier, Righi-Leduc, etc. (see reference [30] for a review). The first measurements of these effects in the mixed phase were performed in the late 1960s [31, 32]. Subsequent to the discovery of high-T_c superconductors in the 1980s, there was also an extensive experimental effort to measure the thermoelectric response of these new exciting materials [33, 34, 35]. In recent years, much of the attention, both theoretically and experimentally, has been focused on the so called *Nernst effect* [36], which is the appearance of a transverse voltage generated by a temperature gradient in a perpendicular magnetic field. While the Nernst effect is very small in the normal state of most metals (bismuth is one prominent exception), it is order of magnitudes larger in the mixed phase of type II superconductors, including the vortex liquid regime of high-T_c superconductors. In this sense, the Nernst effect is an important probe of superconducting fluctuations. The reason for the high level of interest lately is the discovery made some ten years ago of a very large Nernst signal in a special part of the phase diagram of high-T_c hole-doped cuprates [37, 38]. Termed the *pseudogap*, the strange properties of this region is generally believed to hold the key for the understanding of the microscopic mechanisms behind high-T_c superconductivity. Since the pseudogap overlaps with the vortex liquid phase, a possible explanation for the large Nernst signal would be vortex motion [37, 38, 39, 40]. It should be noted, however, that there is certainly no consensus on this matter within the scientific community, and there are plenty of other theories out there, see e.g. [41, 42, 43].

Vortex Nernst effect

On the other hand, in ordinary low-T_c materials, it is established that the dominating contribution to the Nernst signal in the mixed phase comes from mobile vortices. The Nernst coefficient ν and the Nernst signal e_N are defined as

$$\nu = \frac{e_N}{B} = \frac{E_y}{B(-\nabla_x T)}, \tag{1.17}$$

where the electric field E_y is generated by a temperature gradient $\nabla_x T$ and a transverse magnetic field B in the z direction. Let us now, in analogy with the phenomenological description of the generation of a finite electrical resistivity, try to see how vortices can produce such a Nernst signal. Instead of a Lorentz force felt by a vortex in an applied electric current, we can introduce a thermal force per unit length, proportional to the temperature gradient

$$\boldsymbol{F}_t = S_\Phi(-\nabla T), \tag{1.18}$$

and in the direction from hot to cold. The constant of proportionality S_Φ is the *transported entropy* per unit length of a vortex line. This is motivated by the excess entropy of

the normal vortex cores compared to the surrounding superconducting condensate. The excess *configurational* entropy in the hot region, as compared to the cold one, should also be a contributing factor. This latter entropy is essential for coreless vortices, which can be found e.g. in Josephson junction arrays. The thermal motion is in steady state balanced by a friction force $\boldsymbol{F}_f = -\eta \boldsymbol{v}$, giving an average vortex velocity

$$\boldsymbol{v} = S_\Phi(-\nabla T)/\eta. \tag{1.19}$$

These moving vortices generate an electric field $\boldsymbol{E} = -\boldsymbol{v} \times \boldsymbol{B}$ transverse to their motion and to the applied magnetic field, which is the Nernst signal $e_N = v_x B/B(-\nabla_x T) = S_\Phi B/\eta$, assuming the temperature gradient is only in the x direction and the magnetic field of strength B is only in the transverse z direction. Combining Eq. (1.19) with the definition of the Nernst coefficient in Eq. (1.17) we get

$$v_x = \nu(-\nabla_x T). \tag{1.20}$$

This equation makes an important point: The Nernst coefficient ν in Eq. (1.17) is defined as an off-diagonal response, but when generated by vortices the Nernst effect is in fact the *diagonal* response of the vortex velocity to a temperature gradient, and should thus be large. Furthermore, from this description we expect the vortex Nernst coefficient ν to be positive, since vortices move from hotter to colder regions.

One should remember, however, that in reality things can be much more complicated than described in these sections, as vortex motion may be influenced by fluctuations, disorder, interaction effects, etc. For example, in Paper I we show by simulations of a simplistic phase-only model of a 2D superconductor, that the Nernst coefficient ν might in fact be negative under certain circumstances due to geometric frustration.

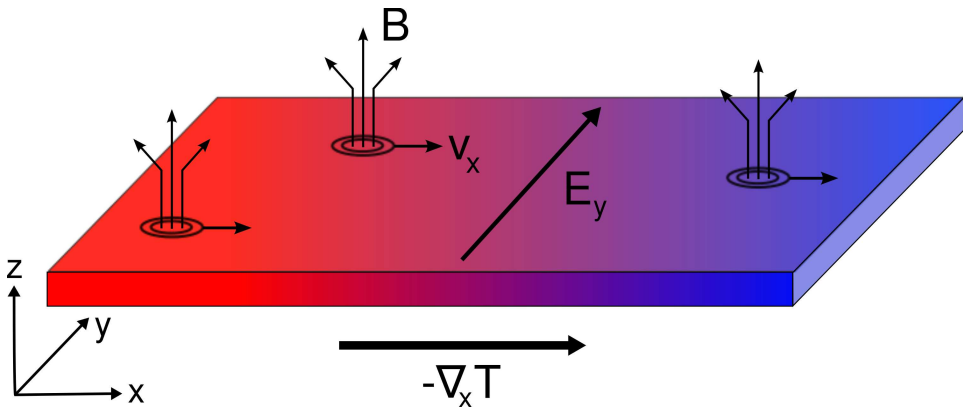

Figure 1.1: In the vortex liquid phase the Nernst signal $e_N = E_y/(-\nabla_x T)$ is dominated by the electric field $\boldsymbol{E} = -\boldsymbol{v} \times \boldsymbol{B} = v_x B$, caused by field induced vortices diffusing down the temperature gradient $-\nabla_x T$ with average velocity v_x.

Chapter 2

Phase fluctuations

Fluctuations in the phase of the superconducting order parameter have a huge impact on the order in low-dimensional systems. Phase fluctuations are also of great importance in high-T_c superconductors, partly due to their quasi-2D structure and partly because of the low density of Cooper pairs in these materials [44]. Another prominent example is a special type of weak link structure, a so called *Josephson junction*, where the phase difference across the junction can drive a tunneling current without an applied voltage, and temporal fluctuations in this phase difference will generate a voltage [45].

We distinguish mainly between two types of phase fluctuations, smooth ones called *spin waves*, and singular *vortex* configurations. Below three dimensions these phase fluctuations drive the average value of the order parameter $\langle\Psi\rangle$ to zero and thus destroy true long range order in the system. While in 1D there is no ordered phase at any nonzero temperature, the limiting 2D case is special. In 2D so called quasi-long range order exists, and the possibility of a phase transition opens up. This transition is the famous *Berezinskii-Kosterlitz-Thouless* (BKT) transition [46, 47], in which vortices play a central role. The starting point for a more detailed description of these matters is naturally the previously introduced phenomenological GL free energy functional. In a fluctuation free mean field approximation, the solution $\Psi_0^2 = -\alpha/\beta$ minimizes the GL free energy in the superconducting phase. To study the effects of phase fluctuations, let us now make the phase of the order parameter position dependent

$$\Psi(\boldsymbol{r}) = \Psi_0 e^{i\theta(\boldsymbol{r})}. \tag{2.1}$$

Inserting this approximation into the GL free energy of Eq. (1.2) we get

$$\begin{aligned} F &= F_n + \int d^d r \left[\alpha\Psi_0^2 + \frac{\beta}{2}\Psi_0^4 + \frac{1}{4m}|(-i\hbar\nabla + 2e\boldsymbol{A})\Psi(\boldsymbol{r})|^2 \right] \\ &= \text{const.} + \int d^d r \, \frac{\hbar^2\Psi_0^2}{4m}(\nabla\theta(\boldsymbol{r}) + \frac{2e}{\hbar}\boldsymbol{A})^2, \end{aligned} \tag{2.2}$$

with the assumption of a constant magnetic induction field $\boldsymbol{B}$. The constant on the last line thus includes the electromagnetic energy, the normal state energy and the contri-

bution from the spatially constant order parameter amplitude. Let us for the moment also ignore the coupling to the vector potential so that the free energy becomes, up to a constant,

$$F = \frac{J_0}{2} \int d^d r (\nabla \theta(\boldsymbol{r}))^2, \tag{2.3}$$

introducing the *superfluid stiffness* $J_0 = \hbar^2 n_s^0 / 4m$, with $\rho_s^0 = 2mn_s^0$ the superfluid density in this phase-only approximation. The name of J_0 is evident from Eq. (2.3): Since F should be minimized, the larger J_0 is, the stiffer the system gets against fluctuations in the phase $\theta(\boldsymbol{r})$. This fact renders phase fluctuations important in materials with small superfluid densities. It is interesting to note that high-T_c superconductors, of both cuprate and ferropnictide type, share this property of small superfluid densities, since these materials are generically insulators and charge carriers therefore have to be introduced by small amounts of doping. Rewriting Eq. (2.3) in Fourier space we have

$$F = \frac{J_0}{2} \int \frac{d^d k}{(2\pi)^d} k^2 |\theta(\boldsymbol{k})|^2, \tag{2.4}$$

where d is the dimensionality of the system. The partition function can be written as a functional integral over all possible phase field configurations

$$Z = \int \mathcal{D}\theta \; e^{-\beta F}. \tag{2.5}$$

Consider now the low temperature regime where fluctuations of θ can be assumed to be small, so that the integration in Eq. (2.5) can be extended to include the entire real line without changing the result. With this, the average of the order parameter is

$$\begin{aligned} \langle \Psi \rangle = \Psi_0 \left\langle e^{i\theta} \right\rangle &= \Psi_0 \int \mathcal{D}\theta \; e^{-\frac{\beta J_0}{2} \int \frac{d^d k}{(2\pi)^d} \left(k^2 |\theta(\boldsymbol{k})|^2 + i\theta(\boldsymbol{k}) \right)} \\ &\sim \Psi_0 \exp\left(-\frac{1}{2\beta J_0} \int_0^\Lambda \frac{d^d k}{k^2} \right), \end{aligned} \tag{2.6}$$

where in the last step the Gaussian functional integral over the phase field was performed. The value of $\langle \Psi \rangle$ depends on the integral in the exponent, which diverges in the thermodynamic limit for $d < 2$, is logarithmically divergent for $d = 2$ and converges for $d > 2$. As a result, $\langle \Psi \rangle = 0$ for $d \leq 2$ for any nonzero temperature, and $\langle \Psi \rangle \neq 0$ for $d = 3$ in the low temperature phase. To see in what sense order is still possible in 2D, let us consider the correlation function

$$g(\boldsymbol{r}) = \langle \Psi(\boldsymbol{r}) \Psi^*(0) \rangle = \Psi_0^2 \left\langle e^{i[\theta(\boldsymbol{r}) - \theta(0)]} \right\rangle = \Psi_0^2 e^{-\frac{1}{2} \left\langle [\theta(\boldsymbol{r}) - \theta(0)]^2 \right\rangle}. \tag{2.7}$$

The second equality stems from a cumulant expansion and the fact that for standard Gaussian distributed variables, all other cumulants vanish. From Eq. (2.4) we obtain

with the help of the equipartition theorem $\frac{1}{2}J_0k^2\left\langle|\theta(k)|^2\right\rangle = \frac{1}{2}k_BT$. With this and by assuming translational invariance

$$-\frac{1}{2}\left\langle[\theta(\boldsymbol{r})-\theta(0)]^2\right\rangle = \frac{1}{\beta J_0}\int\frac{d^dk}{(2\pi)^d}\frac{(e^{i\boldsymbol{k}\cdot\boldsymbol{r}}-1)}{k^2} \approx -\frac{1}{2\pi\beta J_0}\ln(r/a). \tag{2.8}$$

The last step is valid for the 2D case, and a is here a microscopic cutoff, which could for example be the GL correlation length ξ, since the GL theory is only valid on longer length scales. We thus see that the correlation function decays only algebraically to zero at large distances [48]

$$g(r) = \langle\Psi(\boldsymbol{r})\Psi^*(0)\rangle \sim r^{-\eta(T)}, \tag{2.9}$$

with an exponent $\eta(T) = k_BT/2\pi J_0$. The above behavior is known as *quasi-long range order*. Interestingly, this type of power-law decay is also typical of continuous phase transitions, and in that sense $\eta(T)$ can be seen as a temperature dependent critical exponent. In 1D the decay is exponential for all nonzero T, and in 3D the correlation function stays finite as $r \to \infty$, implying true long range order there below T_c. The conclusion that there is no long range order below three dimensions in this model, is a special case of a more general theorem due to Mermin and Wagner [49] and Hohenberg [50].

Eq. (2.9) predicts an algebraic decay of phase correlations at any nonzero temperature. However, at high temperatures, there surely must be a disordered phase signalled by exponentially decaying correlations. One should here remember that the foregoing calculations were done under the assumption of low temperatures, where the phase field fluctuates smoothly in space, i.e., spin-wave fluctuations. If we want to find the advertised phase transition between the two regimes of algebraic and exponential decay, it is thus necessary to consider other types of excitations than just smooth spin waves. These other excitations, that become important at higher temperatures, are singular configurations of the phase field, i.e., vortices. One way to include vortices is to sum also over vortex configurations in the partition function of Eq. (2.5), as will be done in later sections. The *XY model*, described in the upcoming section, represents a second alternative.

2.1 XY model

Being again slightly more general and allowing for a coupling to a fluctuating vector potential $\boldsymbol{A}$, consider the free energy in the phase-only approximation with a constant magnetic induction field $\boldsymbol{B}$ as given by Eq. (2.3). Now discretize space, which amounts to the following substitutions (up to some dimensionally dependent constants)

$$\int d^dr \to \sum_{\langle ij\rangle}, \quad \nabla\theta(\boldsymbol{r}) \to \theta_i - \theta_j, \quad \boldsymbol{A}(\boldsymbol{r}) \to \int_i^j \boldsymbol{A}\cdot d\boldsymbol{r} = A_{ij}, \tag{2.10}$$

where the $\langle ij\rangle$ denotes a sum over all links between nearest neighbor lattice points in the system and A_{ij} is the integrated vector potential over each such link. This gives the

Hamiltonian

$$H = \frac{J_0}{2} \sum_{\langle ij \rangle} (\theta_i - \theta_j - \frac{2\pi}{\Phi_0} A_{ij})^2. \tag{2.11}$$

Here the coupling $J_0 = \hbar^2 \Psi_0^2 / 2m$ is constant, but can in general be taken to vary from link to link. Still we have the same problem as for the continuum case, in that the above Hamiltonian does not reflect an important symmetry of the original order parameter, namely the invariance of a local rotation of the phase with 2π. This invariance is crucial for the existence of vortices. To fix the problem and allow for vortex configurations in the phase field, we choose instead the 2π-periodic cosine function, which also has the correct Taylor expansion to second order. In this way we obtain the XY model Hamiltonian

$$H = -J_0 \sum_{\langle ij \rangle} \cos \left(\theta_i - \theta_j - \frac{2\pi}{\Phi_0} A_{ij} \right). \tag{2.12}$$

The XY model is a prototype model for studying superconductivity, superfluidity, magnetism and many other types of systems in condensed matter physics [51], especially when using numerical simulations. The relation to granular superconductors and Josephson junction systems is discussed in more detail in Paper 1 and 2, where the 2D XY model is employed, with added dynamics, to describe thermoelectric transport properties. In Paper 3 the same model is used for studying scaling of the resistivity at the BKT transition.

2.2 2D Coulomb gas

In the spin-wave analysis at the beginning of this chapter we started from the Gaussian phase-only Hamiltonian

$$H = \frac{J_0}{2} \int d^2 r (\nabla \theta(\boldsymbol{r}))^2, \tag{2.13}$$

and assumed smooth fluctuations of the phase, and thereby neglected vortex configurations. As we saw in Section 1.2, where vortices were specifically introduced as regions of flux penetration in a type II superconductor, the defining mathematical property of a vortex is a nonvanishing and quantized value of the line integral of the phase gradient taken around any path encircling its core

$$\oint \nabla \theta(\boldsymbol{r}) \cdot d\boldsymbol{r} = 2\pi n, \tag{2.14}$$

where n is an integer. By Stokes' theorem we have $\oint d\boldsymbol{r} \cdot \nabla \theta(\boldsymbol{r}) = \int d^2 r \hat{\boldsymbol{z}} \cdot \nabla \times \nabla \theta(\boldsymbol{r})$. Together with the quantization condition above this implies that

$$\nabla \times \nabla \theta(\boldsymbol{r}) = 2\pi \hat{\boldsymbol{z}} \sum_i n_i \delta(\boldsymbol{r} - \boldsymbol{r}_i), \tag{2.15}$$

where the right hand side represents a configuration of vortices with charges n_i at positions $\boldsymbol{r}_i$. Any smooth phase configuration, not showing up as a delta function singularity in the curl of the gradient of the phase, will thus give zero contribution to the circulation in Eq. (2.14). To account for both types of phase fluctuations, we decompose the phase gradient field into two parts

$$\nabla\theta \equiv \boldsymbol{u} = \boldsymbol{u}_{sw} + \boldsymbol{u}_v. \tag{2.16}$$

The part due to spin-wave fluctuations, $\boldsymbol{u}_{sw}$, is curl free, $\nabla \times \boldsymbol{u}_{sw} = 0$, while the vortex part, $\boldsymbol{u}_v$, is divergence free, $\nabla \cdot \boldsymbol{u}_v = 0$. They can therefore be represented as

$$\boldsymbol{u}_{sw} = \nabla\phi, \quad \boldsymbol{u}_v = \nabla \times (\hat{\boldsymbol{z}}\psi) = (\partial_y\psi, -\partial_x\psi, 0), \tag{2.17}$$

giving $\nabla \times \boldsymbol{u}_v = -\hat{\boldsymbol{z}}\nabla^2\psi$. Using this in Eq. (2.15) yields

$$\nabla^2\psi(\boldsymbol{r}) = -2\pi \sum_i n_i \delta(\boldsymbol{r} - \boldsymbol{r}_i). \tag{2.18}$$

This is the familiar Poisson's equation for the potential ψ, in 2D, generated by the vortex charge distribution on the right hand side. The solution is just a superposition of the potentials from each charge, $\psi(\boldsymbol{r}) \approx -\sum_i n_i \ln(|\boldsymbol{r} - \boldsymbol{r}_i|)$, at large distances $|\boldsymbol{r} - \boldsymbol{r}_i|$. With the above decomposition the continuum Gaussian model of Eq. (2.13) becomes

$$H = \frac{J_0}{2}\int d^2r \left[(\nabla\phi)^2 + (\nabla \times (\hat{\boldsymbol{z}}\psi))^2 - 2\nabla\phi \cdot \nabla \times (\hat{\boldsymbol{z}}\psi)\right] = \frac{J_0}{2}\int d^2r \, (\boldsymbol{u}_{sw}^2 + \boldsymbol{u}_v^2), \tag{2.19}$$

where the mixed term vanishes upon integration by parts. The spin-wave and the vortex degrees of freedom thus decouple from each other, $H = H_{sw} + H_v$. The spin-wave part H_{sw} is exactly the Gaussian model analyzed at the beginning of this chapter, and the vortex part can with the help of Eq. (2.18) be simplified

$$H_v = \frac{J_0}{2}\int d^2r \, (\nabla \times (\hat{\boldsymbol{z}}\psi))^2 = -\frac{J_0}{2}\int d^2r \, \psi\nabla^2\psi = 2\pi^2 J_0 \sum_{i,j} n_i n_j V(\boldsymbol{r}_i - \boldsymbol{r}_j), \tag{2.20}$$

where $V(\boldsymbol{r}) \approx -\ln(|\boldsymbol{r}|)/2\pi$ is the *2D Coulomb potential* (the solution to $\nabla^2 V = -\delta(\boldsymbol{r})$). Note here the divergence in the potential at $\boldsymbol{r} = 0$,

$$V(\boldsymbol{r} = 0) = \int_{2\pi/L}^{2\pi/a} \frac{dk}{2\pi}\frac{1}{k} \sim \frac{1}{2\pi}\ln\left(\frac{L}{a}\right) \to \infty, \tag{2.21}$$

coming from the phase-only assumption of a spatially constant amplitude of the order parameter $|\Psi| = \Psi_0$, leading to a delta function charge distribution in Eq. (2.18). This approximation breaks down close to the vortex core, where $|\Psi|$ must go to zero. The divergence as $a \to 0$ implies that the model needs to be regularized at short distances

by imposing a short distance cutoff of the order of the coherence length ξ, to account for the variation of $|\Psi|$ close to the vortex core. This minimum intervortex distance is equivalent to the lattice constant in the XY model. The second divergence, for $L \to \infty$, imposes a *charge neutrality constraint*, $\sum_i n_i = 0$, that makes all divergent terms $i = j$ in Eq. (2.20) cancel each other. With these constraints in place we can write

$$H_v = 2\pi^2 J_0 \sum_{i \neq j} n_i n_j \tilde{V}(\boldsymbol{r}_i - \boldsymbol{r}_j) + E_c \sum_i n_i^2, \tag{2.22}$$

where $\tilde{V}(\boldsymbol{r}) = V(\boldsymbol{r}) - V(0) \approx -\frac{1}{2\pi} \ln(|\boldsymbol{r}|/a)$, with $a \sim \xi$ being the short distance cutoff, and E_c the vortex core energy – simply put the energy cost of creating a vortex in the system. Generally $E_c \sim J_0$, but the exact value of the vortex core energy depends on the details of the cutoff. Finally, we can write the vortex contribution to the total partition function $Z = Z_{sw} Z_v$ for a system of N_+ vortices (charge $n = +1$) and N_- antivortices (charge $n = -1$) as

$$Z_v = \sum_{N_+, N_-} \frac{z^{N_+} z^{N_-}}{N_+! N_-!} \left(\prod_{i=1}^{N} \int \frac{d^2 r_i}{a^2} \right) e^{-\beta H_v}, \tag{2.23}$$

by defining the so called *fugacity* of a vortex as $z = e^{-\beta E_c}$, and $N_+ = N_- = N/2$. With this, we have mapped the phase-only GL free energy to a model with logarithmically interacting charges in two dimensions, the *2D Coulomb gas* model (see e.g. [52] for a review). This is sometimes useful as an alternative to the phase description of the XY model. In Paper 4 we derive an effective action for quantum phase slips in nanowires, and see that the physics of this system at long length scales is essentially that of the 2D Coulomb gas [Eq. (2.23)], but with no neutrality constraint, and a more complicated interaction at short length scales.

2.3 Berezinskii-Kosterlitz-Thouless transition

We now turn to the mechanism behind the alluded phase transition due to vortices in 2D superconducting systems. Berezinskii [46] and Kosterlitz and Thouless [47] (BKT) realized that, in the low temperature phase, vortices and antivortices exist only in neutral tightly bound pairs. At a certain critical temperature, T_{BKT}, these pairs break up and free vortices proliferate and drive the system into an insulating phase with exponentially decaying correlations. This scenario can be understood from a simple argument based on the competition between energy and entropy. The key observation here is that, according to Eq. (2.21), the energy of a single vortex is logarithmically divergent with the system size L

$$E_v \sim \pi J_0 \ln(L/a), \tag{2.24}$$

where we have neglected the finite core energy. On the other hand, a vortex-antivortex pair with separation r has by Eq. (2.22) only a finite energy, $E_{\text{pair}} = \pi J_0 \ln(r/a)$, and

should therefore be the energetically preferable configuration at low temperatures. A thermodynamically stable phase minimizes the free energy

$$F = E - TS, \tag{2.25}$$

where E is the internal energy, T the temperature and S the entropy. The number of places where a single vortex can be located is $(L/a)^2$ and so the entropy is

$$S_v = k_B \ln(L/a)^2. \tag{2.26}$$

The total free energy change due to the introduction of a single vortex in the system is thus in the thermodynamic limit

$$F_v = \pi J_0 \ln(L/a) - 2k_B T \ln(L/a). \tag{2.27}$$

As the temperature increases this changes sign from positive to negative at the BKT critical temperature

$$T_{\mathrm{BKT}} = \frac{\pi J_0}{2k_B}, \tag{2.28}$$

meaning free vortices are stable above this temperature, and thus can give rise to a nonzero resistivity at an arbitrarily small applied electric current. From a more detailed analysis involving a renormalization group (RG) treatment of the problem, it is also possible to see how free vortices destroy the finite superfluid density of the low temperature phase, which jumps discontinuously to zero at $T = T_{\mathrm{BKT}}$. These calculations will be reviewed in the next chapter.

2.4 Josephson junctions

If two superconductors are joined together by a weak link where superconductivity is suppressed, a Josephson junction is formed. The weak link can be realized in several ways [53]: By a thin oxide or normal metal layer, by some type of constriction, point contact, grain boundary, etc. These systems show many fascinating properties in which the phase of the superconducting order parameter plays a key role. Josephson junctions also have many interesting applications in nanoelectronics, as mentioned in the introduction. For example as extremely sensitive magnetometers (SQUIDs) and as candidates for the basic building blocks (qubits) in possible future quantum computers [12], to mention a few.

Josephson effects

The basis for the physics of Josephson junctions are the so called Josephson effects, theoretically predicted by Brian Josephson in 1962 [45]. These effects can be motivated by an elegant derivation due to Feynman [54], which will now be briefly reviewed.

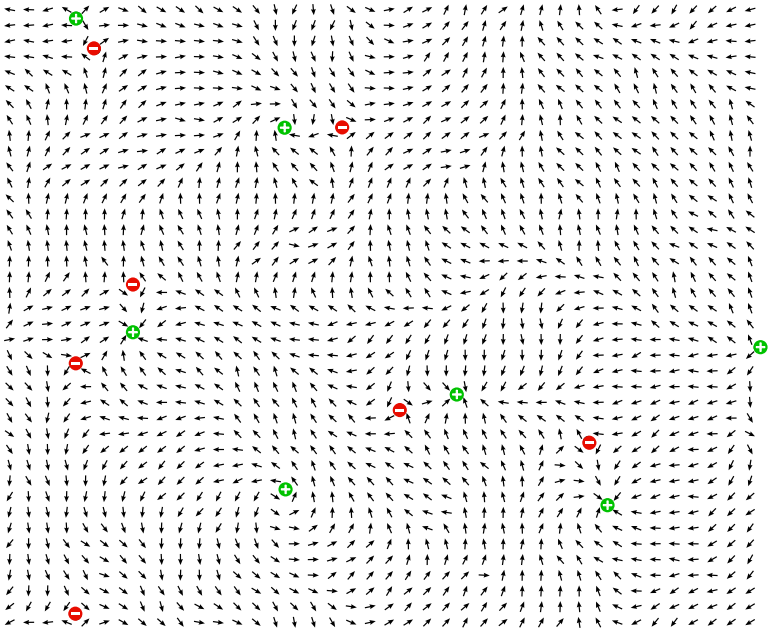

Figure 2.1: Vortex (+) and antivortex (–) configurations in a snapshot from an XY model simulation with periodic boundary conditions in the low temperature phase. Notice how the vortices and antivortices only exist in tightly bound neutral pairs.

Consider a 1D Josephson junction as a system of two superconductors separated by a weak link, thin enough so that the tunneling amplitude of the electron pairs is finite and the two superconductors thus are weakly coupled. The time evolution of the collective wavefunctions $\Psi_{1,2}$, describing the condensed Cooper pairs of each superconductor is then

$$i\hbar\frac{\partial\Psi_{1,2}}{\partial t} = E_{1,2}\Psi_{1,2} + K\Psi_{2,1}, \tag{2.29}$$

i.e, two coupled Schrödinger equations, where K is a coupling parameter, which depends on the nature of the insulating barrier. Suppose now that we apply a constant voltage over the junction giving the potential difference $E_1 - E_2 = 2eV$. By further defining the zero of energy at $(E_1 + E_2)/2$, we get

$$i\hbar\frac{\partial\Psi_{1,2}}{\partial t} = \frac{eV}{2}\Psi_{1,2} \pm K\Psi_{2,1}. \tag{2.30}$$

Rewriting these equations using a polar representation of the complex wavefunctions $\Psi_{1,2} = \sqrt{n_s}e^{i\theta_{1,2}}$, where we assume the same Cooper pair number density n_s in the

two superconductors, the real and imaginary parts can be equated separately to obtain

$$\dot{n}_{1,2} = \pm\frac{2K}{\hbar} n_s \sin(\theta_2 - \theta_1), \tag{2.31}$$

$$\dot{\theta}_{1,2} = \frac{K}{\hbar}\cos(\theta_2 - \theta_1) \pm \frac{eV}{\hbar}. \tag{2.32}$$

The supercurrent from side 1 to 2 is given by $2e\dot{n}_1$ (or $-2e\dot{n}_2$), so Eq. (2.31) tells us that

$$I_s = I_c \sin(\theta_2 - \theta_1), \tag{2.33}$$

where the critical current $I_c = 4en_sK/\hbar$ is the maximum supercurrent the junction can carry before switching to a normal disspative state. For a symmetric junction the critical current is related to the junction normal state resistance R_N and microscopic parameters by the *Ambegaokar-Baratoff formula* [55], $I_c = (\pi\Delta(T)/2eR_N)\tanh(\Delta(T)/2k_BT)$, where $\Delta(T)$ is the superconducting gap. Eq. (2.33) above is the first Josephson equation or the *DC Josephson equation*. It illustrates how the tunneling supercurrent through the junction depends only on the phase difference between the two sides, the so called DC Josephson effect. Note also the resemblance of Eq. (2.33) to the supercurrent from GL theory in Eq. (1.7). The first Josephson equation can in fact be seen as a discrete version of Eq. (1.7), where the sine ensures the 2π addition invariance of the phase of the superconducting order parameter. Subtracting the two equations in Eq. (2.32) gives the second Josephson equation

$$\dot{\theta}_2 - \dot{\theta}_1 = \frac{2e}{\hbar}V, \tag{2.34}$$

expressing that a voltage difference across the junction generates a time dependent phase difference, or conversely that a time dependent phase difference induces a voltage. Integrating this equation and inserting in Eq. (2.33) obtains

$$I = I_c \sin\left(\frac{2e}{\hbar}Vt + \theta_0\right). \tag{2.35}$$

This equation illustrates the *AC Josephson effect* – the presence of a voltage V across the junction generates an oscillating supercurrent with frequency $\nu = \omega/2\pi = 2eV/h = V/\Phi_0$. The relation directly links frequency to voltage through fundamental constants, thus providing a possible voltage standard.

As we have seen before, in a magnetic field the phase difference must be *gauge-invariant* and therefore changes from $\theta_2 - \theta_1$ to $\theta_2 - \theta_1 - (2\pi/\Phi_0)\int_2^1 \boldsymbol{A}\cdot d\boldsymbol{r} = \gamma$ in the Josephson relations above. Actually, the second Josephson equation [Eq. (2.34)] can in a sense be seen as a result of the gauge invariance, as it is simply obtained by taking the time derivative of γ, while recognizing that $\boldsymbol{E} = -\dot{\boldsymbol{A}}$. Using the Josephson relations [Eq. (2.33) and Eq. (2.34)] in their gauge-invariant forms, the electric energy stored in a Josephson junction can be calculated as

$$u = \int I_s V dt = \int \frac{\hbar I_c}{2e}\dot{\gamma}\sin(\gamma)dt = -\frac{\hbar I_c}{2e}\cos\left(\theta_i - \theta_j - \frac{2\pi}{\Phi_0}A_{ij}\right), \tag{2.36}$$

which is exactly on the form of the energy of a link from a site i to a site j in the XY model [Eq. (2.12)] with a coupling $E_J = \hbar I_c/2e$. The coupling constant E_J is in this context referred to as Josephson coupling energy.

Josephson junction arrays

Connecting several Josephson junctions together into a network, one gets what is known as a *Josephson junction array* (JJA) [56, 57, 58]. In light of the previous discussion we see that a 2D JJA is a physical representation of the 2D XY model, and so the same physics dicussed in this chapter, like the BKT transition, applies also for JJAs. Furthermore, since JJAs are artificially created systems, where various system parameters can be controlled, they provide an excellent testing ground for theoretical models. This has lead to an interesting cross-fertilization between theory and experiment. Granular superconducting thin films are closely related to arrays of Josephson junctions. In these films superconducting grains of different sizes are connected by Josephson junctions, with various critical currents I_c, depending on the contact between them. These systems can be modeled by disordered JJAs. In Paper 1 and 2 we study the transport properties of models of geometrically disordered JJAs, much like one displayed in Fig. 2.2.

The physics of JJAs is especially rich in a transverse magnetic field, where vortex structure and dynamics are important. Vortices in JJAs are somewhat different from vortices in bulk superconductors. Instead of forming in the superconducting material itself, they sit in the spaces between the superconducting islands, since this saves some condensation energy, and screening supercurrents flow as tunneling currents in the junctions around them. As a consequence, vortex formation is possible not only in JJAs made of type II superconductors, but also in those fabricated using type I materials. At weak magnetic fields the vortex density in the array is low and the average vortex separation is much larger than the lattice spacing. For low fields one therefore expects that the effects due to the discreteness of the array are negligible and that the JJA can be used as a model for a continuous type II superconductor. However, as the applied magnetic field strength is increased, vortices start to interact with the underlying lattice. At special vortex densities or fillings $f = \Phi/\Phi_0$ the corresponding vortex lattice is particularly symmetric, making it unusually stable against thermal fluctuations. This will have a dramatic effect on transport properties, since vortices suddenly might become pinned as the magnetic field is varied through one of these special values, causing for example the resistance to almost vanish. In perfectly symmetric arrays these effects are most pronounced, while they still exist but are smoothened out in slightly disordered systems such the one in Fig. 2.2.

These effects, in connection with simulations of electrical resistivity, thermal conductivity, and the Nernst effect, are discussed in some detail in Paper 1 and 2.

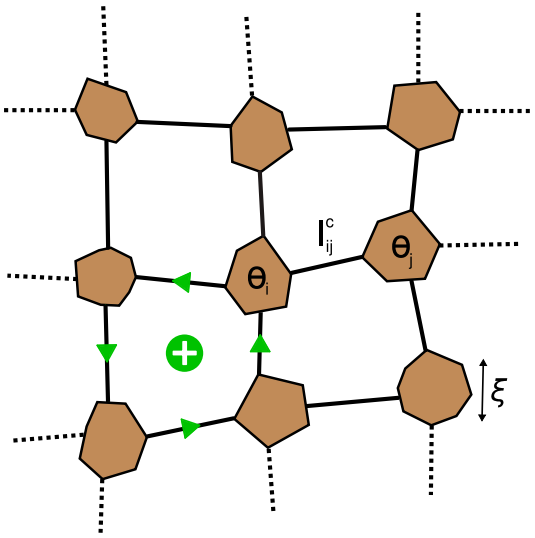

Figure 2.2: A geometrically disordered 2D Josephson junction array may serve as a model for a granular superconductor. Grains are of size less than the coherence length ξ, so that the phase θ_i of each grain is well defined. These grains are connected by Josephson junctions, whose critical current is I^c_{ij}. The green dot illustrates a vortex in the array with supercurrents flowing in the junctions surrounding it.

2.5 Phase slips

In the foregoing sections we have seen how a temporal fluctuation in the phase difference γ across a Josephson junction generates an instantaneous voltage $V = \hbar\dot{\gamma}/2e$. Fluctuations of this type are called *phase slips* and may be either thermal or quantum-mechanical in nature. Phase slips are key in the basic understanding of both Josephson junctions and thin superconducting wires.

We start by considering purely classical thermal phase slips. For this we need a dynamical description of a Josephson junction. One such possible description is provided by the resistively and capacitively shunted Josephson junction *(RCSJ) model*. In this model the Josephson junction is shunted by a capacitor C and a resistor R, where the capacitor simply reflects the capacitance of the junction itself, and the resistor accounts for normal current tunneling and possible current leakage (see Fig. 4.2 in Chapter 4, where the RCSJ model for a Josephson junction array of arbitrary geometry is described). For simplicity the resistor is assumed to be ohmic. Now, if the junction is connected to an external current source with current I, this current will be the sum of these three

parallel channels

$$I = I_c \sin\gamma + \frac{V}{R} + C\dot{V} = I_c \sin\gamma + \frac{\hbar}{2eR}\dot{\gamma} + C\left(\frac{\hbar}{2e}\right)^2 \ddot{\gamma}, \tag{2.37}$$

where in the second step the second Josephson equation was inserted. The solution of this differential equation is best described by considering its mechanical analog, which is a particle of mass $C(\hbar/2e)^2$ moving along the γ coordinate in an effective potential

$$U(\gamma) = -E_J \cos\gamma - \frac{\hbar}{2e} I\gamma, \tag{2.38}$$

and subjected to a friction force $\dot{\gamma}(\hbar/2e)^2/R$ [7]. The potential, often referred to as the *tilted washboard potential*, is plotted in Fig. 2.3 for different values of the bias current I. The tilt of the washboard is controlled by the bias current. For $I = 0$ the particle is trapped in one of the local minima of the cosine potential, corresponding to zero average voltage and a superconducting state. For currents $I > I_c$ the tilt makes the minima disappear and the particle starts to move, giving a finite voltage normal state. When decreasing the bias current again, the particle will be retrapped at some current less than the critical current, depending on the competition between the effects of friction and inertia. This description crudely reflects the basic current-voltage characteristics seen in experiments on Josephson junctions. Considering also thermal fluctuations in the current through the resistor, gives the particles a chance to overcome the potential barriers, producing phase slips of 2π in either direction. However, in absence of any bias current, the rates of forward and backward thermally activated slips of the phase difference γ are equal, and so the time averaged voltage is still zero. For $I \neq 0$, on the other hand, this is not the case, since the height of the forward and backward barriers then differ, $\Delta U_\pm = 2E_J \pm (2\pi\hbar/2e)I$, giving phase slip rates of $\dot{\gamma}_\pm \sim e^{-\Delta U_\pm/k_B T}$. The time average of the Josephson voltage is proportional to the net phase slip rate $\dot{\gamma}_+ - \dot{\gamma}_-$, which in the limit of small currents gives an effective resistivity [7]

$$\rho \sim e^{-2E_J/k_B T}, \tag{2.39}$$

in analogy with the vortex creep phenomena in bulk superconductors described by Eq. (1.16). This description essentially applies to thin superconducting bulk wires as well, since the coarse-grained description of these are one-dimensional chains of Josephson junctions. The main difference lies in that the absence of tunneling junctions in bulk wires, requires the amplitude of the superconducting order parameter to vanish at the point of the phase slip. This costs some condensation energy. The typical volume where the amplitude is suppressed is of the order of $s\xi$, where s is the wire's cross-sectional area and ξ the coherence length. This leads for a small bias currents to a resistance on the same thermal activation form as in Eq. (2.39), but now with an energy barrier height $\Delta E \sim s\xi f_0$, where $f_0 = \alpha^2/4\beta$ is the condensation energy per unit volume from the GL functional in Eq. (1.2). These calculations based on GL theory, of *thermally activated phase slips* (TAPS) in superconducting bulk wires, were done in the late 1960s by

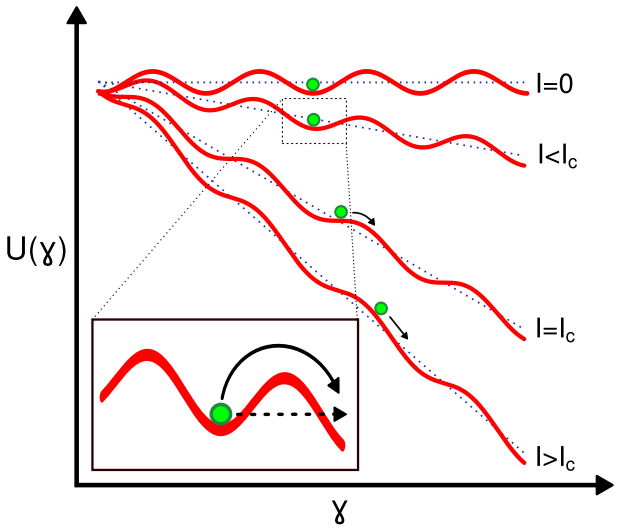

Figure 2.3: A particle with mass $C(\hbar/2e)^2$ subjected to a friction force $\dot{\gamma}(\hbar/2e)^2/R$ moving along the coordinate γ in the tilted washboard potential $U(\gamma)$ is the mechanical analog of the RCSJ model in Eq. (2.37). The bias current I determines the tilt of the potential. Inset: The particle can make a transition from one minima to another (corresponding to a phase slip of 2π) either by thermal activation over the barrier or by quantum tunneling through the barrier.

Little [59], Langer and Ambegaokar [60], and McCumber and Halperin [61]. The theory was soon confirmed in experiments on thin Sn wires [62, 63] and by many other subsequent measurements.

Quantum phase slips

At low temperatures quantum effects come into play. In terms of the tilted washboard picture in Fig. 2.3, this presents the possibility of quantum tunneling through the potential barrier, instead of thermal activation over it, i.e., a *quantum phase slip* (QPS). In principle, this means that superconductivity can be destroyed for all temperatures including $T \to 0$, if the QPS are sufficiently instense, so called coherent QPS [64].

The first signs of QPS in superconducting wires were reported on by Giordano [65]. He found an upturn of the resistivity far below T_c in thin ($\sim$0.5 μm) In wires, which could not be accounted for using the TAPS description. Even more clear-cut evidence for the existence of QPS in wires, is provided by a number of recent experiments on ultrathin MoGe [66, 67, 68, 69] and Al [70, 71] wires. These wires can be made extremely thin, with diameters down to below 10 nm. This is shorter than the coherence length ξ in these materials, meaning they are effectively one-dimensional. A theory of QPS processes in uniform quasi-1D superconducting wires has been developed by Golubev

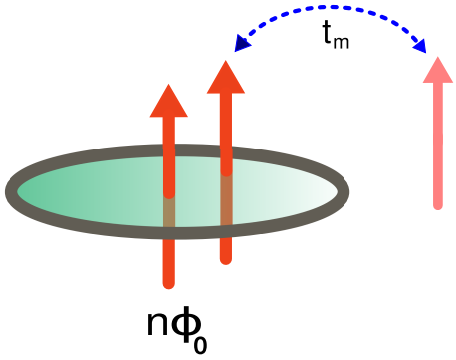

Figure 2.4: A superconducting nanowire ring. A quantum phase slip event corresponds here to the tunneling of a flux quantum Φ_0 (or many) in or out of the ring. An effective quantum-mechanical Hamiltonian for this system is given by Eq. (2.40).

and Zaikin and coworkers [72, 73, 74]. In contrast to theoretical approaches based on Ginzburg-Landau theory (which only should be trusted close to T_c) the theory remains applicable in the limit $T \to 0$, and also claims to properly account for non-equilibrium, dissipative and electromagnetic effects during a QPS event [74].

At low temperatures the quantum state of a long superconducting wire, where the ends have been connected to form a loop, can be specified by the number of flux quanta n inside the loop. Neglecting any geometric self-inductance of the loop, the ground state energy is a periodic pattern of crossing parabolas with period Φ_0. In analogy with the description in a Josephson junction, a quantum phase slip here corresponds to the tunneling between minima in this energy landscape, i.e., the quantum tunneling of a flux quantum Φ_0 in or out of the loop (see Fig. 2.4). A QPS changes the flux through the ring and thus generates a voltage pulse, leading to dissipation. In the limit when QPS are abundant in the wire, the coherent QPS process of flux tunneling across the wire shows a facinating duality to the classical Josephson effect, i.e., the transport of a Cooper pair from one end of the wire to the other. This duality opens up for future technological applications of QPS circuits, similar to those based on Josephson junctions [75].

One can write an effective quantum-mechanical Hamiltonian, taking into account QPS processes, of a thin superconducting wire loop as [76]

$$H = \sum_n E_0 \left|n\right\rangle \left\langle n\right| - \sum_{n,m} t_m (\left|n+m\right\rangle \left\langle n\right| + \left|n\right\rangle \left\langle n+m\right|), \tag{2.40}$$

where t_m couples flux states differing in flux by $m\Phi_0$. In other words, t_m is the probability amplitude for a QPS event in which m flux quanta tunnel simultaneously in or out of the loop. In Paper 4 we consider this system and show how t_m can be obtained. We are also able to calculate t_m through computer simulations based on a reformulation of the microscopic effective action for QPS derived by Golubev and Zaikin.

Chapter 3

Renormalization and scaling

Paper 3 of this thesis is devoted to the study of scaling at the BKT transition. Renormalization group flow equations for the superfluid stiffness and the fugacity are used as an important tool in this analysis. We here present an explicit derivation of those flow equations for the 2D Coulomb gas model, introduced in the last chapter. As a warmup for this calculation, we start by discussing the main ideas behind the renormalization group, along with some general scaling theory at continuous phase transitions. The chapter concludes with a brief summary of the topic of quantum phase transitions, and the interesting correspondence between quantum and classical systems – all of which is highly relevant for the modeling of quantum phase slips done in Paper 4.

Scaling analysis lies at the heart of any study of phase transitions. It enables extraction of information about the way different physical quantities behave close to *continuous phase transitions*, i.e., phase transitions where the order parameter goes continuously to zero at the critical point, as opposed to *first order* or *discontinuous phase transitions*, e.g., the melting of ice into water. This behavior of quantities such as the order parameter, specific heat, or susceptibility, is quantified by *critical exponents*, describing the power-law decay or divergence of these observables close to criticality. Amazingly, the same critical exponents show up in many seemingly unrelated physical systems. This fact is called *universality*. Through a concept known as the *renormalization group* (RG), introduced in statistical physics by Kadanoff [77] in 1966 and further developed and refined mathematically by Wilson [78, 79] a couple of years later, we can understand the critical scaling properties of physical observables and the universality of these properties (see e.g. [51, 80, 81] for more complete discussions on this issue).

3.1 Basic ideas of RG

While the fancy name could certainly lead you to think so, the way the renormalization group (RG) is used in physics, is often neither general, nor is it exact. Rather it should be viewed more as a concept, whose implementation can look very different from case

to case.

In this spirit let us walk through the main steps and ideas of an RG transformation. Precisely at the critical point of a continuous phase transition the correlation length ξ diverges and becomes infinite. At this point the system shows a *fractal* nature, meaning that one finds fluctuations at all length scales. When changing perspective and zooming in to look closer at the system, things will thus appear exactly the same. The system has become *scale-invariant*. Kadanoff's original idea [77] that lead to the birth of RG theory was to make use of this scale invariance by systematically integrating out degrees of freedom on short length scales $\boldsymbol{\Psi}_<$, giving an effective Hamiltonian H' in terms of the remaining long length-scale degrees of freedom $\boldsymbol{\Psi}_>$

$$e^{-\beta H'[\boldsymbol{\Psi}_>]} = \int \mathcal{D}\boldsymbol{\Psi}_< e^{-\beta H[\boldsymbol{\Psi}_<, \boldsymbol{\Psi}_>]}. \tag{3.1}$$

This step is known as *coarse-graining*. The art of RG is really to find a clever coarse-graining procedure that works for the problem at hand. Practically this can be achieved in a multitude of ways, e.g., through a blocking procedure in real space suggested by Kadanoff [77], or by following Wilson [79] and integrating out short wavelength modes in Fourier space. One should mention that, usually, this step is very hard and sometimes involves some sort of uncontrolled approximation. Note that the coarse-graining changes the minimum length scale in the system from a to ba, where $b > 1$ is the scaling factor. To regain the same resolution as before, the second step is to *renormalize* or rescale all lengths

$$\boldsymbol{r}' = \boldsymbol{r}/b. \tag{3.2}$$

It might also be necessary to renormalize the remaining degrees of freedom $\boldsymbol{\Psi}_> \to \boldsymbol{\Psi}'$. The final step is to exploit the scale invariance concept by demanding the statistical weights of the renormalized system $e^{-\beta H'[\boldsymbol{\Psi}']}$ to be on the same form as the old ones $e^{-\beta H[\boldsymbol{\Psi}]}$. This can be achieved by renormalization of the parameters in the reduced Hamiltonian $\beta H'$, $(K_1, K_2, ...) = \boldsymbol{K} \to \boldsymbol{K}'$. Iteration of this RG transformation will cause a flow of these parameters in the space spanned by them, known as an *RG flow*. Often new interactions are also generated. In each RG transformation the correlation length is reduced $\xi[\boldsymbol{K}'] = \xi[\boldsymbol{K}]/b$, and so in all systems which are off criticality and therefore has a finite ξ, the flow ultimately goes towards the *fixed point* $\xi(\boldsymbol{K}^*) = 0$, corresponding to complete disorder at high temperatures, or complete order at low temperatures. A critical system, on the other hand, has $\xi(\boldsymbol{K}_c) = \infty$, and is thus infinitely scale-invariant. In this way the RG flow of any set of starting parameters $\boldsymbol{K}$ is towards the fixed point $\boldsymbol{K}^*$, that defines the true long length-scale physics of that starting set.

The RG flow in the vicinity of a critical fixed point determines the critical exponents of the corresponding phase transition. But only a certain number of the variables in $\boldsymbol{K}$ grow in size during each RG iteration, and these will determine the faith of the flow close to a critical fixed point and drive all off critical systems away from this point. These are called *relevant* variables, whereas the others are called *irrelevant* (if they decrease under RG the transformation) or marginal (if they stay constant).

For a critical fixed point that corresponds to an ordinary continuous phase transition, there are usually two relevant scaling variables, the temperature and the variable conjugate to the order parameter. This fact, i.e., that only a few variables of all the possible in $\boldsymbol{K}$ drive the flow close to a critical fixed point, is one way to understand the universality of the critical exponents.

3.2 Scaling

If the summing of the Boltzmann weights over configurations of short length-scale degrees of freedom (in order to obtain the renormalized weights in Eq. (3.1)) can be done exactly (an exact RG transformation), the partition function is unchanged

$$Z = \int \mathcal{D}\boldsymbol{\Psi} e^{-\beta H[\boldsymbol{\Psi}]} = \int \mathcal{D}\boldsymbol{\Psi}' e^{-\beta' H'[\boldsymbol{\Psi}']} = Z'. \tag{3.3}$$

This defines how the reduced free energy density $f = \beta F/V$ transforms under an RG procedure

$$f(\boldsymbol{K}) = -\frac{\ln Z}{V} = -\frac{\ln Z'}{V' b^d} = b^{-d} f(\boldsymbol{K}'). \tag{3.4}$$

Close to a critical fixed point we may write this in terms of, say, two relevant scaling variables k_1 and k_2, while ignoring the irrelevant ones, giving the *free energy homogeneity law*

$$f(k_1, k_2, ...) = b^{-d} f(k_1 b^{y_{k_1}}, k_2 b^{y_{k_2}}, ...), \tag{3.5}$$

where we have assumed that the scaling variables transform as $k_i' = k_i b^{y_{k_i}}$, with y_{k_i} an unknown exponent. This assumption is motivated by the fact that two successive RG transformations with scale factor b and b' must give the same result as one transformation with scale factor bb', and also that setting $b = 1$ should change nothing, $\boldsymbol{K}' = \boldsymbol{K}$. Considering a case where the reduced temperature $t = |T - T_c|/T_c$ is the only relevant variable, the correlation length, on the other hand, transforms simply as

$$\xi(t) = b\xi(t b^{y_t}) = t^{-1/y_t} \xi(1) \sim t^{-1/y_t}, \tag{3.6}$$

where the arbitrary scale factor $b = t^{-1/y_t}$ in the second step. Now, since ξ diverges as

$$\xi \sim t^{-\nu} \tag{3.7}$$

at criticality $t \to 0$, we obtain the connection $\nu = 1/y_t$. Using the same trick as above, the scaling form of other static thermodynamic quantities and the connection between the scaling exponents y_{k_i} and the critical exponents of these quantities follow by simple differentiation of Eq. (3.5).

As a result of the diverging correlation length, the typical time scale of fluctuations, the correlation time τ, also diverges at a continuous phase transition

$$\tau \sim \xi^z, \tag{3.8}$$

which defines the *dynamic critical exponent* z. The critical properties of dynamic quantities, such as the resistivity, are determined by z. It is also of great importance in the analogy between quantum and classical phase transitions, as will be evident in a later section. In Paper 3, the difficulty of determining z at the BKT transition plays a leading part in the story.

The dynamic critical exponent naturally depends on the equations of motions of choice, and as a result, the same effective Hamiltonian could display different values of z. However, z still shows universality, in that it only depends on basic symmetries and conservation laws of the specific dynamical equation [82].

Finite size scaling

In numerical simulations the system size L is by necessity finite, and thus acts a cutoff for the diverging correlation length ξ close to criticality. The inverse system size L^{-1} should therefore be included as a relevant scaling variable in the transformation of the singular part of the free energy

$$f(t, L^{-1}) = b^{-d} f(tb^{1/\nu}, L^{-1}b). \tag{3.9}$$

The value of L^{-1} must, just as the reduced temperature $t = (T - T_c)/T_c$, tend to zero in order to reach the critical point, i.e., this happens only in the thermodynamic limit $L \to \infty$. By choosing $b = L$ we obtain the very convenient finite size scaling form

$$f(t, L^{-1}) = L^{-d} f(tL^{1/\nu}, 1). \tag{3.10}$$

As an example of the practical use of this form, one could for example exploit that $f \sim L^{-d}$ at the critical temperature $t = 0$, and use this to find T_c from the intersection point of curves of $L^d f$ vs T for different system sizes L. Alternatively one could also try to determine the critical exponent ν by collapsing curves of $L^d f$ vs T for different L in the critical region. Usually some quantity other than the free energy is used to do this analysis.

3.3 BKT transition: RG equations and scaling

To obtain RG flow equations for the BKT transition within the 2D Coulomb gas model, we start from the linear response result that the superfluid stiffness can be written as [51]

$$J = J_0 \left(1 - \beta J_0 \lim_{k \to 0} \frac{1}{\Omega k^2} \langle n(\boldsymbol{k}) n(-\boldsymbol{k}) \rangle \right), \tag{3.11}$$

where $J_0 = \hbar^2 n_s^0/4m$ is the *bare* superfluid stiffness in Eq. (2.3), Ω is the system volume, and $n(\boldsymbol{k})$ is the Fourier transform of the vortex charge distribution $n(\boldsymbol{r}) = 2\pi \sum_i n_i \delta(\boldsymbol{r} - \boldsymbol{r}_i)$ defined by Eq. (2.18). For small k we may expand the vortex density correlation function as [83]

$$\begin{aligned} n(\boldsymbol{k})n(-\boldsymbol{k}) &= (2\pi)^2 \sum_{i,j} n_i n_j e^{-i\boldsymbol{k}\cdot(\boldsymbol{r}_i - \boldsymbol{r}_j)} \\ &\approx (2\pi)^2 \sum_{i,j} n_i n_j \left(1 - i\boldsymbol{k}\cdot(\boldsymbol{r}_i - \boldsymbol{r}_j) - \frac{1}{2}[\boldsymbol{k}\cdot(\boldsymbol{r}_i - \boldsymbol{r}_j)]^2\right), \end{aligned} \tag{3.12}$$

where the zeroth order term vanishes because of the neutrality constraint $\sum_i n_i = 0$. The idea is now to consider low temperatures $k_B T \ll E_C$, where the vortex fugacity $z = e^{-\beta E_c}$ is small, and the 2D Coulomb gas partition function in Eq. (2.23) can be expanded in orders of z. To second order in z, it is enough to consider the trivial configuration with no vortices, $N = 0$, and the one with a single neutral vortex-antivortex pair, $N = 2$,

$$Z_v \approx 1 + z^2 \int_{|\boldsymbol{r}_1 - \boldsymbol{r}_2| > a} \frac{d^2 r_1}{a^2} \frac{d^2 r_2}{a^2} \left(\frac{|\boldsymbol{r}_1 - \boldsymbol{r}_2|}{a}\right)^{-\pi\beta J_0}. \tag{3.13}$$

Using this form of the partition function, it is straightforward to calculate the ensemble average of the vortex charge correlation function $\langle n(\boldsymbol{k})n(-\boldsymbol{k})\rangle$. The first order term in k in Eq. (3.12) vanishes upon integration over the spatial coordinates, while the second order term gives a contribution

$$\langle n(\boldsymbol{k})n(-\boldsymbol{k})\rangle = \Omega k^2 2\pi^3 z^2 \int_a^\infty \frac{dr}{a} \left(\frac{r}{a}\right)^{3 - 2\pi\beta J_0}, \tag{3.14}$$

where we have used that $az^2/(1+bz^2) = az^2 + \mathcal{O}(z^4)$, so the partition function $Z_v = 1$ to order z^2 in this expression. Insertion of this result in Eq. (3.11) yields

$$J = J_0 - \beta J_0^2 2\pi^3 z^2 \int_a^\infty \frac{dr}{a} \left(\frac{r}{a}\right)^{3 - 2\pi\beta J_0}, \tag{3.15}$$

which to second order in z can be rewritten as

$$\frac{1}{K} = \frac{1}{K_0} + 2\pi^3 z^2 \int_a^\infty \frac{dr}{a} \left(\frac{r}{a}\right)^{3 - 2\pi K_0}, \tag{3.16}$$

with $K = \beta J$ and $K_0 = \beta J_0$ being dimensionless superfluid stiffnesses. The integral in this expression diverges and drives K to zero unless $3 - 2\pi K_0 < -1$, which gives $T < \pi J_0/2k_B$, the same critical temperature as in Eq. (2.28), found from the simple energy-entropy argument.

By applying some type of renormalization procedure it is possible to extract more information from the integral. Kosterlitz [84] did this by studying how the dimensionless

superfluid stiffness changes when incrementally increasing the lower cutoff in the integral $a \to ae^{d\ell}$. One neat way to make this analysis is to break the integral in Eq. (3.16) into two pieces [85]

$$\frac{1}{K} = \frac{1}{K'} + 2\pi^3 z^2 \int_{ae^{d\ell}}^{\infty} \frac{dr}{a} \left(\frac{r}{a}\right)^{3-2\pi K_0}, \tag{3.17}$$

where the short distance part of the integral goes into the renormalized stiffness K' defined by

$$\frac{1}{K'} = \frac{1}{K_0} + 2\pi^3 z^2 \int_{a}^{ae^{d\ell}} \frac{dr}{a} \left(\frac{r}{a}\right)^{3-2\pi K} = \frac{1}{K_0} + 2\pi^3 z^2 \frac{e^{(4-2\pi K_0)d\ell} - 1}{4 - 2\pi K_0}. \tag{3.18}$$

By now rescaling the integration variable $r \to re^{-d\ell}$ we get back to the same form as in Eq. (3.15), but with a *renormalized stiffness* K' given by Eq. (3.18), and a *renormalized fugacity* z' defined by

$$z' = ze^{(2-\pi K_0)d\ell}. \tag{3.19}$$

Taking the limit $d\ell \to 0$, these relations give to lowest order in fugacity the differential RG equations of the BKT transition as

$$\frac{dK^{-1}(\ell)}{d\ell} = 2\pi^3 z^2(\ell), \quad \frac{dz}{d\ell} = [2 - \pi K(\ell)]z(\ell), \tag{3.20}$$

where $K(\ell = 0) = K_0$ and $z(\ell = 0) = z = e^{-\beta E_c}$, and $\ell = \ln b$ is the logarithm of some scale factor b. The critical fixed point of this RG flow is $(K^*, z^*) = (2/\pi, 0)$, which gives almost the same critical condition as in Eq. (2.28), $J/k_B T_{\text{BKT}} = 2/\pi$, but now with the renormalized stiffness J instead of the bare one J_0.

To get the RG flow equations on a nicer form it is convenient to introduce the reduced stiffness variable $x = (K^* - K)/K^*$ and the fugacity variable $y = 2\pi z$. Close to the fixed point we can expand to lowest order in x and y to get

$$\frac{dx(\ell)}{d\ell} = y^2(\ell), \quad \frac{dy}{d\ell} = 2x(\ell)y(\ell). \tag{3.21}$$

By direct integration of these the solution $x^2(\ell) - y^2(\ell) = c$ is obtained, with $c = x^2(\ell_0) - y^2(\ell_0)$ being a constant that depends on the intial values of x and y. The flow of x and y with increasing ℓ is illustrated in Fig. 3.1. The region $c > 0$ is easily discerned to be the low temperature phase, where the flow is towards zero fugacity $y = 0$ and nonzero reduced stiffness $x = -\sqrt{c} = -\sqrt{x^2(\ell_0) - y^2(\ell_0)}$, entirely decided by the starting point. The entire line $x < 0$ is thus a line of fixed points. By inserting the fully renormalized ($\ell \to \infty$) stiffness K into the correlation function of Eq. (2.9), we conclude that the low temperature phase is characterized by *quasi-long range order* $g(r) \sim r^{-\eta}$, with an exponent $\eta = 1/(2\pi K) = 1/4$ at T_{BKT} (since $K(T \to T_{\text{BKT}}^-) = 2/\pi$), and which decreases for lower temperatures. For $c < 0$ the flow is first towards smaller

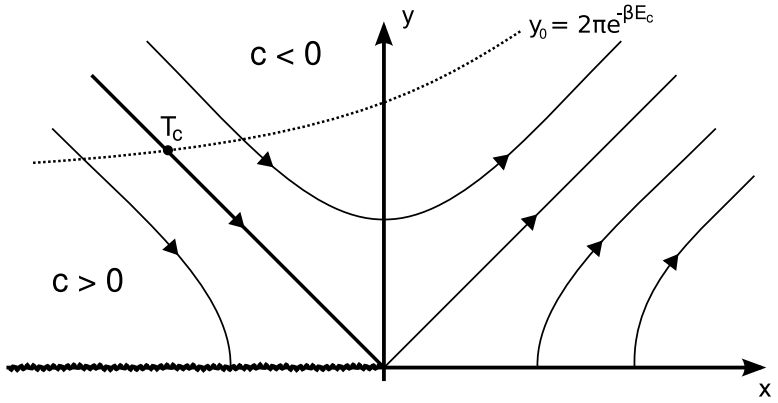

Figure 3.1: Sketch of the RG flow [Eq. (3.20)] of the fugacity y and the reduced phase stiffness x, close to the BKT critical point $(x, y) = (0, 0)$. The dotted line is a line of starting points for the flow, given by the bare fugacity $y_0 = 2\pi e^{-\beta E_c} = e^{-cK_0} \sim e^x$. To the left of the separatrix $x = y$, the flow ends in the line of fixed points $y = 0$, $x < 0$ (marked by the wiggly line).

fugacities, but $y(\ell)$ soon turns upwards and tends to infinity just as $x(\ell)$ does for large ℓ, i.e., we end up in the high temperature phase with vanishing stiffness and exponentially decaying correlations. These two regions are separated by the line $c = 0$ and $y = -x$, which flows into the critical fixed point $(x^*, y^*) = (0, 0)$. We conclude that c measures the closeness to the phase transition, i.e., we must have $c = c_0^2(T_{\text{BKT}} - T)$, with c_0 some constant.

From the explicit solutions [52] of Eq. (3.21) the correlation length is found to have an unusual *exponential divergence*

$$\xi \sim e^{1/\sqrt{|c|}} \sim e^{1/c_0\sqrt{|T_{\text{BKT}}-T|}}. \tag{3.22}$$

Below the critical temperature, ξ can be thought of as the size of the largest vortex-antivortex pair in the system, whereas it above T_{BKT} sets the density of free vortices $n_F \sim 1/\xi_+^2$ (or the size of the largest thermally stable vortex-antivortex pair). Depending on the precise definition of ξ, the value of the constant in the exponent can vary and is generally different above and below T_{BKT}. Note also that since the divergence of ξ from Eq. (3.22) is faster than any power law, ν is effectively infinite at the BKT transition.

One other prominent ramification of this RG flow is that the superfluid stiffness renormalizes to a constant $K \to 2/\pi$ as $T \to T_{\text{BKT}}^-$, while $K \to 0$ as $T \to T_{\text{BKT}}^+$, meaning that the superfluid stiffness parameter K drops from $2/\pi$ to 0 at $T = T_{\text{BKT}}$. The size of this jump of the superfluid stiffness is a universal hallmark [86] for all systems experiencing a BKT transition, and has been experimentally verified in helium-4 films [87] as well as in thin-film superconductors [88].

3.4 Quantum phase transitions

A quantum phase transition (QPT) is a transition between different ground states of a system, as a parameter other than the temperature is varied. Strictly speaking, quantum effects are always important on small enough length scales or at low enough temperatures and may alter the classical description. However, since the correlation length ξ and time scale τ of typical long length-scale fluctuations of the order parameter diverge close to a continuous phase transition, the corresponding energy scale vanishes as $\hbar\omega \sim |T - T_c|^{\nu z}$, according Eqs. (3.7) and (3.8). For a phase transition at a finite temperature T_c, this energy scale will be small compared to the thermal energy $k_B T_c$, and quantum effects become negligible close to the critical point for $t < T_c^{1/\nu z}$ [89]. This means that a true quantum phase transition, where quantum effects determine the critical exponents, can only happen at zero temperature, but also that quantum fluctuations might still be important for nonuniversal properties close to a classical finite temperature phase transition.

Nevertheless, there exists a remarkable mapping between the quantum statistical mechanics of a d-dimensional system and classical statistical mechanics in $d+1$ dimensions, which enables the study of quantum phase transitions by analysis of their higher dimensional classical counterparts. An example of this approach given in Paper 4, where the microscopic quantum description of a superconducting quasi-1D nanowire is rephrased in terms of a classical $(1+1)$D gas of vortex charges interacting in space-time, closely related to the 2D Coulomb gas.

Quantum-classical correspondence and scaling

The partition function $Z = \mathrm{Tr} e^{-\beta H}$ contains all equilibrium information about a system. In quantum mechanics the time evolution operator is $e^{-iHt/\hbar}$, which is equal to the canonical density operator $e^{-\beta H}$ in imaginary time $\tau = \hbar\beta = it$. In terms of a complete set of states, the partition function is

$$Z = \int dn \left\langle n \left| e^{-\beta H} \right| n \right\rangle , \tag{3.23}$$

i.e., a sum over transition amplitudes of a system starting in some state $|n\rangle$ and evoling for $-i\hbar\beta$ in imaginary time, and then returning to the same state again. This implies that to obtain the static equilibrium properties of a quantum system, one must also solve for the dynamics. This is rooted in the noncommutative nature of the position and momentum operators. The mapping from quantum to classical is provided by Feynman's *path integral* formulation of quantum mechanics, where the imaginary time evolution is broken up into a large number of incremental time steps $e^{-\beta H} = \left[e^{-(\Delta\tau/\hbar)H}\right]^N$, with $N\Delta\tau = \hbar\beta$. By also inserting sums over complete sets of states, $\int dn \, |n\rangle \langle n| = 1$,

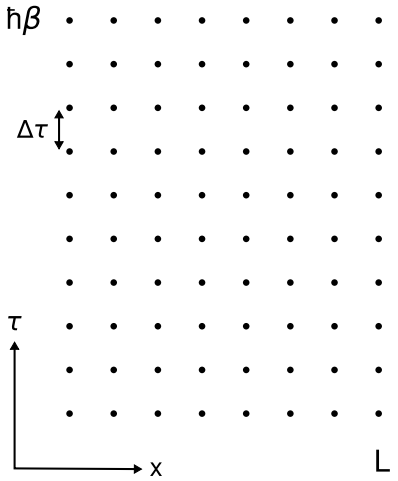

Figure 3.2: Discrete $L \times \hbar\beta$ space-time lattice, corresponding to a 1D quantum system of length L at a finite temperature. There are always periodic boundary conditions in the time dimension, due to the trace in the partition function.

between each time slice, the partition function becomes

$$Z = \int dn_1 dn_2 ... dn_N \left\langle n_1 \left| e^{-(\Delta\tau/\hbar)H} \right| n_2 \right\rangle \left\langle n_2 \left| e^{-(\Delta\tau/\hbar)H} \right| n_3 \right\rangle \times ... \\ ... \times \left\langle n_N \left| e^{-(\Delta\tau/\hbar)H} \right| n_1 \right\rangle . \quad (3.24)$$

The time evolution operators couple system configurations at different times with each other, and so imaginary time acts as an additional dimension. If the complete sets of states are chosen to be appropriate eigenstates (often position and momentum) to operators in the Hamiltonian, Eq. (3.24) can be transformed into a completely *classical* partition function with sums running over the eigenvalues of these operators [90]. Starting with, say, a 1D quantum system of length L, the corresponding classical system will be a $(1+1)$D space-time system of size $L \times \hbar\beta$ (see Fig. 3.2). Nonzero temperature (finite β) thus corresponds to a finite time dimension. Note also that the original trace in Eq. (3.23) enforces periodic boundary conditions in the time direction. Evident from this mapping is also that the classical scaling of the free energy in Eq. (3.5) has to be modified somewhat close to a QPT. Since the correlation time diverges as $\tau \sim \xi^z$ at criticality, the dynamic critical exponent z expresses the space-time anisotropy at a QPT. Many systems have $z = 1$ and thus an isotropically diverging correlation volume $\xi^d \times \xi^z$, but in general z is different from one [91]. Consequently, the free energy homogeneity law at a quantum phase transition can be written as [89, 92]

$$f(k, T, ...) = b^{-(d+z)} f(kb^{1/\nu}, Tb^z, ...), \quad (3.25)$$

where the nonthermal reduced parameter $k = |K - K_c|/K_c$, and the finite temperature T are both relevant scaling variables. We see that this is analogous to the scaling at a classical continuous phase transition, given by Eq. (3.5), but here in $d + z$ dimensions. This equation provides the basis for the scaling analysis at a QPT. For instance, it is used in Paper 4 to scale the quantum phase slip amplitude, which has the dimension of energy, and therefore, according to Eq. (3.25), scales with finite system size (in the spatial dimension) as $\sim L^{-z}$ at criticality $K = K_c$.

Chapter 4

Dynamical models and simulation methods

In the course of work behind this thesis we employ mainly two different categories of simulation methods: Ones based on stochastic differential equations, and so called Monte Carlo methods.

In Paper 1, 2 and 3 we study transport coefficients. These reflect *nonequilibrium* dynamical properties of the system. In this case the time evolution of the simulations should preferably stay close to the physical reality. Two such possible types of dynamics that we use are Langevin dynamics and resistively and capacitively shunted Josephson junction (RCSJ) dynamics. These are represented by *stochastic differential equations* (SDE), which can be solved numerically on a computer by some clever discretization of time derivatives, and with the help of pseudo-random numbers. When time evolution is unimportant, and only *equilibrium* quantities need to be sampled, *Monte Carlo* (MC) methods are useful. Just like an SDE, a Monte Carlo method generates a wanted statistical distribution using pseudo-random numbers, but is generally more effective, since the dynamics can be chosen almost arbitrarily. In Paper 3, a cluster Monte Carlo scheme, called the Wolff algorithm, is employed to effectively reduce the equilibration time at criticality, after which the Langevin or RCSJ dynamics are used to sample transport properties. In Paper 4 we use a grand canonical Monte Carlo scheme, where the total number of particles in the system is allowed to fluctuate, to simulate quantum phase slips in thin superconducting wires.

The aim of this chapter is to present briefly some generalities about numerical integration of stochastic differential equations and Monte Carlo methods, and more importantly, to give an in-depth review of the specific implementations of these methods in our simulations.

4.1 Stochastic differential equations

The archetypal stochastic differential equation in physics is an overdamped *Langevin equation* on the form

$$\gamma\dot{\theta}(x,t) = f[\theta(x,t)] + \zeta(x,t), \tag{4.1}$$

where θ is some generalized coordinate of the system, γ a friction coefficient, f a deterministic force, and ζ a stochastic force term. This type of equation can be coupled, on purely phenomenological grounds, to any statistical mechanics model described by a Hamiltonian H, by setting the deterministic force $f = -\partial H/\partial\theta$, so that the rate at which the system relaxes towards the local energy minimum is proportional to the deviation from it. Of course, one of the more basic properties of any dynamical equation is to converge the system towards some appropriate target distribution, from which sampling of observables can be made. The clever way to do this is to choose the target distribution to be the same as the distribution one wants to sample, especially if the sampling distribution is very peaked, as is indeed the case for the canonical Boltzmann distribution $p_i = e^{-\beta H_i}/Z$. This approach is called *importance sampling* [93].

To achieve convergence to some equilibrium distribution p_i, one must require two things. First, an equilibrium distribution is a stationary distribution, meaning that the sum of all transition rates in and out of a state i must be equal,

$$\sum_i p_j P(j \to i) = \sum_i p_i P(i \to j), \tag{4.2}$$

where $P(i \to j)$ is the transition probability to go from state i to state j. The second requirement is *ergodicity*, i.e., the state space must not contain any isolated states, so that the equilibrium distribution can be reached from any state the system happens to traverse. By simply choosing the transition probabilities according to the *detailed balance* condition,

$$p_i P(i \to j) = p_j P(j \to i), \tag{4.3}$$

the target distribution p_i becomes stationary, as Eq. (4.2) is obviously fulfilled. For the ergodicity requirement, on the other hand, there is no general solution. When designing a new update method, one must therefore explicitly make sure that ergodicity is satisfied. Assuming it is, it is possible to show that detailed balance will make the system converge to the wanted target distribution in the limit of many update steps [93]. Note, however, that the rate at which equilibrium is approached strongly depends on the specific system at hand, the update method used, and the closeness to criticality.

Functional integral representation

Let us now see what this means for our overdamped Langevin equation

$$\gamma\dot{\theta}(x,t) = -\frac{\partial H[\theta]}{\partial\theta} + \zeta(x,t), \tag{4.4}$$

where we take the stochastic term to be locally correlated in space and time

$$\langle \zeta(x,t)\zeta(x',t')\rangle = A\delta(x-x')\delta(t-t'), \tag{4.5}$$

and Gaussian distributed,

$$P[\zeta] \sim e^{-\frac{1}{2A}\int dxdt\ \zeta^2(x,t)}. \tag{4.6}$$

The trick here is to use the functional integral resolution of unity [90, 94]

$$1 = \int \mathcal{D}\zeta\ \delta[\theta - \theta_{\text{sol}}] = \int \mathcal{D}\zeta D\tilde{\theta}\ e^{i\int dxdt(\gamma\dot{\theta}+\frac{\partial H[\theta]}{\partial\theta}-\zeta)\tilde{\theta}}, \tag{4.7}$$

where the delta functional $\delta[\theta - \theta_{\text{sol}}] = \delta[\dot{\theta} + \frac{\partial H[\theta]}{\partial\theta} - \zeta]$ enforces $\theta(t)$ to solve Eq. (4.4). Inserting this into Eq. (4.6) and performing the functional integrals over the stochastic noise ζ and the help variable $\tilde{\theta}$, gives the probability of a path $\theta(t)$ on the *Onsager-Machlup* form [95]

$$P[\theta(t)] \sim e^{-S[\theta]}J[\theta], \qquad S[\theta] = \frac{1}{2A}\int dxdt\left(\gamma\dot{\theta} + \frac{\partial H[\theta]}{\partial\theta}\right)^2, \tag{4.8}$$

with $J[\theta] = |\det(\delta\zeta/\delta\theta)|$, a Jacobian from the change of variables $\zeta \to \theta$, obtained by evaluation of the functional integrals over ζ and $\tilde{\theta}$. The value of $J[\theta]$ depends on the explicit time discretization used. This functional integral (or path integral) formulation is quite useful as an alternative description of a stochastic differential equation, in this case Eq. (4.4). In Paper 2 we use this approach to motivate the form of the Kubo formula for the Nernst signal.

We are now in a position to write down the transition probability of an incremental update from state i with $\theta(t)$ to state j with $\theta(t+dt)$ using Eq. (4.4). We have

$$\begin{aligned}\frac{P(i\to j)}{P(j\to i)} &= \frac{e^{-\frac{1}{2A}\int dx\int_t^{t+dt} dt\left(\gamma\dot{\theta}+\frac{\partial H}{\partial\theta}\right)^2}}{e^{-\frac{1}{2A}\int dx\int_t^{t+dt} dt\left(-\gamma\dot{\theta}+\frac{\partial H}{\partial\theta}\right)^2}} \\ &= e^{-\frac{1}{A}\int dx\int_t^{t+dt} dt\left(\gamma\dot{\theta}\frac{\partial H}{\partial\theta}\right)} = e^{-\frac{2\gamma}{A}[H(t+dt)-H(t)]}.\end{aligned} \tag{4.9}$$

The conclusion here is that to satisfy the detailed balance condition of Eq. (4.3) with an equilibrium Boltzmann distribution $p_i \sim e^{-\beta H_i}$, the stochastic noise strength constant A from Eq. (4.5) must depend on both the temperature and the friction coefficient,

$$A = 2\gamma/\beta = 2\gamma k_B T. \tag{4.10}$$

4.2 Numerical solution of SDEs

A stochastic differential equation can be solved on a computer in much the same way as a deterministic equation, namely by discretization of time in units of Δt. The general

overdamped Langevin equation in Eq. (4.1) is readily discretized by a simple *forward Euler* approximation of the time derivative

$$\dot{\theta}(t) = \frac{1}{\Delta t}[\theta(t + \Delta t) - \theta(t)], \tag{4.11}$$

giving the integration scheme

$$\theta(t + \Delta t) = \theta(t) + \frac{\Delta t}{\gamma}\left[f[\theta(t)] + \zeta(t)\right]. \tag{4.12}$$

Here care must be taken considering the stochastic term, which is delta function correlated in time, $\langle \zeta(t)\zeta(t')\rangle = A\delta_{tt'}$. Since we want to preserve the defining property of the delta function also in the discrete case

$$\int dt\; g(t)\delta(t - t') = g(t') \quad \rightarrow \quad \sum_t g_t \hat{\delta}(t - t')\Delta t = g_{t'}, \tag{4.13}$$

it is necessary to define the discrete version of the delta function as $\hat{\delta}(t - t') = \delta_{tt'}/\Delta t$, where $\delta_{tt'}$ is the Kronecker delta. This leads to an update scheme

$$\theta(t + \Delta t) = \theta(t) + \frac{\Delta t}{\gamma}\left[f[\theta(t)] + \sqrt{A/\Delta t}\,\zeta(t)\right], \tag{4.14}$$

where now $\langle \zeta(t)\zeta(t')\rangle = \delta_{tt'}$, which can be satisfied if ζ is a random number drawn from a Gaussian distribution with zero mean and unit variance. Note also that the noise term goes as $\sqrt{\Delta t}$, making the error in each update step $\mathcal{O}(\Delta t)$ instead of $\mathcal{O}((\Delta t)^2)$ as in the deterministic case [81, 96].

The RCSJ dynamics equation of motion is essentially on the form of a general Langevin equation, which can be obtained by restoring the inertial term in Eq. (4.1)

$$m\ddot{\theta}(t) = -\gamma\dot{\theta}(t) + f[\theta(t)] + \zeta(t). \tag{4.15}$$

This is second order in time, but can be rewritten as two first order equations

$$m\dot{v}_\theta(t) = -\gamma v_\theta(t) + f[\theta(t)] + \zeta(t), \tag{4.16}$$

$$\dot{\theta}(t) = v_\theta(t). \tag{4.17}$$

A nice way to integrate these on a computer is provided by the *leap frog* scheme [97]. This algorithm evaluates the velocity variables on half-integer time steps, giving the time derivative of the velocity variable at integer time steps as

$$\dot{v}_\theta(t) = \frac{1}{\Delta t}\left[v_\theta\left(t + \frac{\Delta t}{2}\right) - v_\theta\left(t - \frac{\Delta t}{2}\right)\right]. \tag{4.18}$$

The velocity variable is then used to update the coordinate variables defined only on integer time steps. The full scheme looks like

$$v_\theta\left(t+\frac{\Delta t}{2}\right) = v_\theta\left(t-\frac{\Delta t}{2}\right) + \frac{\Delta t}{m}\left[-\gamma v_\theta(t) + f[\theta(t)] + \sqrt{\frac{A}{\Delta t}}\zeta(t)\right], \tag{4.19}$$

$$\theta(t+\Delta t) = \theta(t) + \Delta t\, v_\theta\left(t+\frac{\Delta t}{2}\right). \tag{4.20}$$

Since the velocity variable itself is not defined at integer time steps, it must be calculated as the average of velocities at adjacent half-integer time steps

$$v_\theta(t) = \frac{1}{2}\left[v_\theta\left(t+\frac{\Delta t}{2}\right) + v_\theta\left(t-\frac{\Delta t}{2}\right)\right]. \tag{4.21}$$

There is a notable difference between the forward Euler scheme of Eq. (4.12) and the leap frog algorithm of Eqs. (4.19) and (4.20). Leap frog has the nice property of being fully symmetric (and therefore time reversible) in the sense that $\dot{\theta}(t)$ and $\dot{v}_\theta(t)$ are calculated by evaluation of quantities at the midpoint of the time step. The forward Euler scheme, on the other hand, is clearly asymmetric in the same sense, since the evaluation in this case is at the beginning of the time step. Although this might seem like a small difference, the two discretizations can actually lead to different results, even in the limit of a small time step $\Delta t \to 0$. This is sometimes called the *Ito-Stratonovich dilemma* [98, 99], where Ito discretization refers to the asymmetric rule of forward Euler, and Stratonovich discretization to the symmetric one used in the leap frog scheme.

In Paper 2 we indeed notice this dilemma. We there find that the heat current is sensitive to the discretization scheme, and that in order to obtain self-consistent results it is necessary to adopt the symmetric Stratonovich discretization. This is automatically done when using RCSJ dynamics with leap frog, while for Langevin dynamics with forward Euler, the heat current expression must be symmetrized.

4.3 Langevin dynamics

The system we intend to describe is a 2D granular superconductor or Josephson junction network of size $L \times L$, with or without geometric disorder, placed in a uniform transverse magnetic field (see Fig. 2.2 for a possible realization of this). As discussed previously, this system is characterized by the XY model Hamiltonian

$$H = -\sum_{\langle ij\rangle} J_{ij}\cos\left(\theta_i - \theta_j - \frac{2\pi}{\Phi_0}A_{ij}\right). \tag{4.22}$$

In our model the magnetic vector potential is decomposed into two parts, one space dependent and one time dependent, $\boldsymbol{A}(\boldsymbol{r},t) = \boldsymbol{A}_{\text{ext}}(\boldsymbol{r}) + \frac{\Phi_0}{2\pi}\boldsymbol{\Delta}(t)$. The space dependent term generates the uniform transverse magnetic field $\bar{\boldsymbol{B}} = \nabla \times \boldsymbol{A}_{\text{ext}}$, while the other one

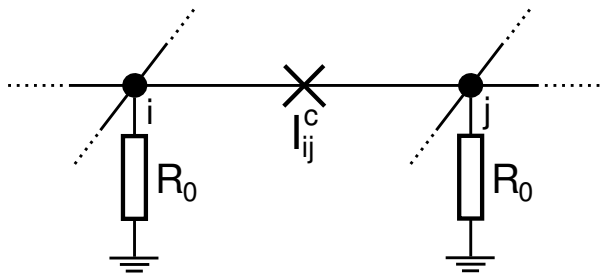

Figure 4.1: The electric circuit equivalent to Langevin dynamics.

describes temporal fluctuations in the average electric field $\bar{\boldsymbol{E}} = -\frac{\Phi_0}{2\pi}\dot{\boldsymbol{\Delta}}$. The dynamic $\boldsymbol{\Delta}$ variable also describes the phase twist per unit length in the system, and is therefore known as *fluctuating twist boundary conditions* (FTBC) [100]. These allow us to use periodic boundary conditions and at the same time measure a voltage across the system. We further make the gauge choice $\boldsymbol{A}_{\text{ext}}(\boldsymbol{r}) = Bx\hat{\boldsymbol{y}}$, giving $\bar{\boldsymbol{B}} = B\hat{\boldsymbol{z}}$, which leads to an integrated magnetic vector potential

$$A_{ij} = \int_{\boldsymbol{r}_i}^{\boldsymbol{r}_j} \boldsymbol{A} \cdot d\boldsymbol{r} = By_{ji}x_{ij}^c + \boldsymbol{\Delta} \cdot \boldsymbol{r}_{ji}, \tag{4.23}$$

where $\boldsymbol{r}_{ji} = \boldsymbol{r}_j - \boldsymbol{r}_i$ is the vector from grain i to grain j, y_{ji} the y component of this vector, and $x_{ij}^c = (x_i + x_j)/2$ the midpoint in the x direction.

Following the prescription outlined in a previous section, the simplest dynamical equations for the phases $\{\theta_i\}$ and the twist variable $\boldsymbol{\Delta}$ are of relaxational Langevin type

$$\gamma\dot{\theta}_i = -\frac{1}{\hbar}\frac{\partial H}{\partial \theta_i} + \eta_i, \qquad \gamma_\Delta\dot{\boldsymbol{\Delta}} = -\frac{1}{\hbar}\frac{\partial H}{\partial \boldsymbol{\Delta}} + \boldsymbol{\zeta}, \tag{4.24}$$

where the stochastic terms $\{\eta_i\}$ and $\boldsymbol{\zeta}$ are white noise correlated and Gaussian with zero mean and with a variance proportional to the temperature. These equations of motion essentially represent time-dependent Ginzburg-Landau (TDGL) [101] equations for a phase-only description provided by the XY model Hamiltonian in Eq. (4.22).

Alternatively, we can think of these equations as describing the dynamics of a network of electrical circuit elements, shown in Fig. 4.1, where each site i is connected to a resistor R_0 to ground

$$\gamma\dot{\theta}_i = \frac{V_i}{2eR_0} = -\frac{1}{2e}\sum_{j\in\mathcal{N}_i} I_{ij}^s + \eta_i, \quad \gamma_\Delta\dot{\boldsymbol{\Delta}} = \frac{1}{2e}\left(\sum_{\langle ij\rangle} I_{ij}^s \boldsymbol{r}_{ji} - L^2\bar{\boldsymbol{J}}^{\text{ext}}\right) + \boldsymbol{\zeta}, \tag{4.25}$$

where $I_{ij}^s = I_{ij}^c \sin(\theta_i - \theta_j - \frac{2\pi}{\Phi_0}A_{ij})$ is the tunneling supercurrent from grain i to grain j, through a Josephson junction with critical current $I_{ij}^c = 2eJ_{ij}/\hbar$. The equation of motion for the phases $\{\theta_i\}$ can in this description be derived from current conservation

at each grain i

$$\sum_{j\in\mathcal{N}_i} I_{ij}^s + \frac{\hbar}{2eR_0}\dot{\theta}_i + I_i^n = 0, \tag{4.26}$$

where the sum runs over the set $\mathcal{N}_i$ of grains connected to grain i, $V_i = \hbar\dot{\theta}_i/2e$ is the Josephson voltage to ground over the resistor R_0, and I_i^n is the *Johnson-Nyquist noise* current [102, 103] in this resistor, with properties $\langle I_i^n(t)\rangle = 0$ and $\langle I_i^n(t)I_j^n(t')\rangle = (2k_BT/R_0)\delta_{ij}\delta(t-t')$. Regrouping the above equation gives exactly the equation of motion for the phases in Eq. (4.25), and also relates the dimensionless time constant with the ground resistance through $\gamma = \hbar/4e^2R_0$. To arrive at the dynamics for $\boldsymbol{\Delta}$, imagine adding a resistance R_0 in parallel with the entire array in both directions. By fixing the average total current $L\bar{\boldsymbol{J}}_{\text{ext}}$, which is a sum of the total supercurrent in the junctions, the current through the parallel resistor, and the noise current in that resistor, we get

$$L\bar{\boldsymbol{J}}^{\text{ext}} = \frac{1}{L}\sum_{\langle ij\rangle} I_{ij}^s \boldsymbol{r}_{ji} - \frac{\hbar}{2eR_0}L\dot{\boldsymbol{\Delta}} + I^n, \tag{4.27}$$

being the equation of motion for $\boldsymbol{\Delta}$, if we make the identification $\gamma_\Delta = \gamma L^2 = L^2\hbar/4e^2R_0$. This way of describing Langevin dynamics might seem a bit strange at first, but serves a purpose, since it allows for a comparison with the more realistic RCSJ dynamics (described in the upcoming section), which is in fact based on a circuit description of a network of Josephson junctions.

Implementation-wise, the Langevin equations of motion, Eq. (4.25), are trivial to handle due to their simple structure, and can be integrated as they stand. Our simulations employ the forward Euler time discretization scheme of Eq. (4.12). Note that most of the CPU time in a simulation is used to calculate the sums in the right-hand side of both equations in Eq. (4.25). By exploiting the fact that these sums can be done independently, the algorithm is easy to parallelize almost perfectly.

4.4 RCSJ dynamics

Consider again the 2D granular superconductor depicted in Fig. 2.2. In addition to the tunneling supercurrent through the Josephson junctions connecting the grains, it is natural to assume displacement currents through the proximity induced capacitances between grains. If we also consider the possibility of normal electron tunneling and current leakage through the junctions, accounted for by the introduction of some parallel resistance, we arrive at the RCSJ model [104, 105]. The basic circuit element of a network of such junctions is shown in Fig. 4.2. We subsequently write the total current from grain i to grain j as

$$I_{ij}^{\text{tot}} = I_{ij}^c \sin\gamma_{ij} + \frac{V_{ij}}{R} + C\dot{V}_{ij} + I_{ij}^n \equiv I_{ij}^s + I_{ij}^r + I_{ij}^C + I_{ij}^n, \tag{4.28}$$

where the Josephson voltage $V_{ij} = \frac{\hbar}{2e}\dot{\gamma}_{ij} = \frac{\hbar}{2e}(\dot{\theta}_i - \dot{\theta}_j - \frac{2\pi}{\Phi_0}\dot{A}_{ij})$, and the thermal noise current in the parallel resistor has zero mean and covariance $\langle I_{ij}^n(t)I_{kl}^n(t')\rangle =$

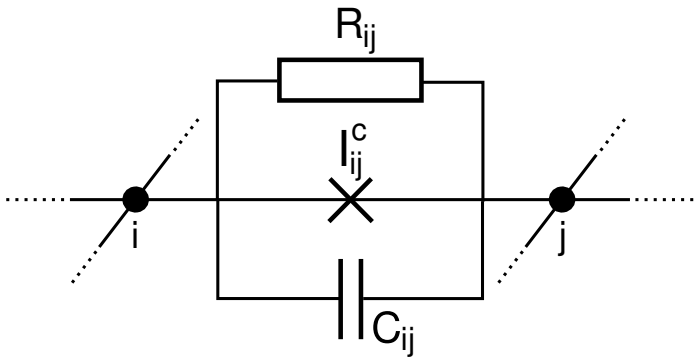

Figure 4.2: The electric circuit equivalent to RCSJ dynamics.

$(2k_BT/R)(\delta_{ik}\delta_{jl}-\delta_{il}\delta_{jk})\delta(t-t')$. Measuring time in units of $\hbar/2eRI^c$ and temperature in units of $\hbar I^c/2ek_B$ Eq. (4.28) can be rewritten as

$$I_{ij}^{\rm tot} = I_{ij}^c \sin\gamma_{ij} + \dot{\gamma}_{ij} + Q^2\ddot{\gamma}_{ij} + I^n = I_{ij}^s + I_{ij}^r + I_{ij}^C + I_{ij}^n, \tag{4.29}$$

with $Q^2 = 2eR^2I^cC/\hbar = \beta_c$, a dimensionless parameter introduced by Stewart [104] and McCumber [105], who where the first to study this model. The parameter Q^2 is the ratio between the two time scales RC and $\hbar/RI^c$ and controls the damping. For large values of Q the inertial term (the capacitance current) is important and the system is considered underdamped, while it is overdamped for small Q. In the fully overdamped limit $Q \to 0$ one obtains the RSJ model, without the parallel capacitance in Fig. 4.2.

Demanding the total current to be conserved at each grain and fixing the average current in the system

$$\sum_{j\in\mathcal{N}_i} I_{ij}^{\rm tot} = 0, \qquad \sum_{\langle ij\rangle} I_{ij}^{\rm tot}\boldsymbol{r}_{ji} = L^2\bar{\boldsymbol{J}}^{\rm ext}, \tag{4.30}$$

generates equations of motion for the phases $\{\theta_i\}$ and the twists $\boldsymbol{\Delta}$. In the first of these equations the sum is taken over the set of all junctions $\mathcal{N}_i$ connected to each grain i. The second equation can be understood from the definition of the current density $\boldsymbol{J}(\boldsymbol{r})$ living only on the links of the lattice

$$\boldsymbol{J}(\boldsymbol{r}) = \sum_{\langle ij\rangle}\int_{\boldsymbol{r}_i}^{\boldsymbol{r}_j} I_{ij}^{\rm tot}\delta(\boldsymbol{r}-\boldsymbol{r}')d\boldsymbol{r}'. \tag{4.31}$$

Fixing the system average of this current density, $\frac{1}{L^2}\int dr^2\boldsymbol{J}(\boldsymbol{r}) = \bar{\boldsymbol{J}}^{\rm ext}$, gives directly

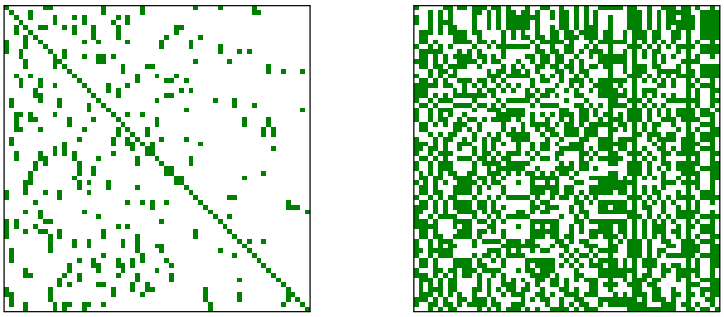

Figure 4.3: An example of a discrete Laplacian matrix D (left) for a disordered lattice. D is always sparse, while the inverse D^{-1} (right) is typically dense. The green elements are nonzero.

the second relation in Eq. (4.30). The explicit form of the dynamical equations are

$$\sum_{j\in\mathcal{N}_i}(\ddot{\theta}_i-\ddot{\theta}_j)-(\sum_{j\in\mathcal{N}_i}\boldsymbol{r}_{ji})\cdot\ddot{\boldsymbol{\Delta}}=-\frac{1}{Q^2}\sum_{j\in\mathcal{N}_i}(I^s_{ij}+I^r_{ij}+I^n_{ij}), \tag{4.32}$$

$$\sum_{\langle ij\rangle}(\ddot{\theta}_i-\ddot{\theta}_j)\boldsymbol{r}_{ji}-(\sum_{\langle ij\rangle}\boldsymbol{r}_{ji}\boldsymbol{r}^T_{ji})\ddot{\boldsymbol{\Delta}}=\frac{L^2}{Q^2}\bar{\boldsymbol{J}}^{\text{ext}}-\frac{1}{Q^2}\sum_{\langle ij\rangle}(I^s_{ij}+I^r_{ij}+I^n_{ij})\boldsymbol{r}_{ji}. \tag{4.33}$$

Notice the relatively complicated structure of these equations compared to the Langevin dynamics equations of motion, Eq. (4.25), stemming from the extra constraint of current conservation, which for Langevin dynamics in practice is relaxed by the resistors R_0 to ground.

In preparation for the numerical integration, we proceed by rewriting Eqs. (4.32) and (4.33) as two first order differential equations on matrix form

$$\begin{bmatrix} D & -\lambda \\ \lambda^T & -\omega \end{bmatrix}\begin{bmatrix}\dot{\boldsymbol{v}}_\theta \\ \dot{\boldsymbol{v}}_\Delta\end{bmatrix}=\frac{1}{Q^2}\begin{bmatrix}\boldsymbol{a}\\ \boldsymbol{b}\end{bmatrix},\qquad \begin{bmatrix}\dot{\boldsymbol{\theta}}\\ \dot{\boldsymbol{\Delta}}\end{bmatrix}=\begin{bmatrix}\boldsymbol{v}_\theta\\ \boldsymbol{v}_\Delta\end{bmatrix}. \tag{4.34}$$

Here D is minus the *discrete Laplacian* matrix, defined by $D_{ij}f_i=\sum_{j\in\mathcal{N}_i}(f_i-f_j)$, or $D_{ij}=|\mathcal{N}_i|\delta_{i=j}-\delta_{j\in\mathcal{N}_i}$, with one row and one column removed to avoid it being singular. (The singularity is a consequence of the fact that the equations of motion are invariant under a global rotation of the phases [106].) For a system of $L\times L=N$ sites, D is thus an $(N-1)\times(N-1)$ matrix, while the $2\times(N-1)$ matrix $\lambda^T=\sum_{j\in\mathcal{N}_i}\boldsymbol{r}_{ji}$ is obtained using the relation $\sum_{\langle ij\rangle}(\dot{\theta}_i-\dot{\theta}_j)\boldsymbol{r}_{ji}=\sum_i\dot{\theta}_i\sum_{j\in\mathcal{N}_i}\boldsymbol{r}_{ji}$ in Eq. (4.33), and further the 2×2 matrix $\omega=\sum_{\langle ij\rangle}\boldsymbol{r}_{ji}\boldsymbol{r}^T_{ji}$. The right hand side of Eq. (4.34) is simply given by the column vectors $a_i=-\sum_{j\in\mathcal{N}_i}(I^s_{ij}+I^r_{ij}+I^n_{ij})$ and $\boldsymbol{b}=L^2\bar{\boldsymbol{J}}^{\text{ext}}-\sum_{\langle ij\rangle}(I^s_{ij}+I^r_{ij}+I^n_{ij})\boldsymbol{r}_{ji}$. From here we can apply the leap frog discretization of $\dot{\boldsymbol{v}}_{\theta,\Delta}$ and $\boldsymbol{v}_{\theta,\Delta}$ introduced in Eqs. (4.18) and (4.21), which after some straightforward algebra leads to

the update scheme

$$\begin{bmatrix} D & -\lambda \\ \lambda^T & -\omega \end{bmatrix} \begin{bmatrix} \frac{a}{d}\boldsymbol{v}_\theta\left(t+\frac{\Delta t}{2}\right) + \frac{b}{d}\boldsymbol{v}_\theta\left(t-\frac{\Delta t}{2}\right) \\ \frac{a}{d}\boldsymbol{v}_\Delta\left(t+\frac{\Delta t}{2}\right) + \frac{b}{d}\boldsymbol{v}_\Delta\left(t-\frac{\Delta t}{2}\right) \end{bmatrix} = \frac{1}{Q^2}\begin{bmatrix} \boldsymbol{A} \\ \boldsymbol{B} \end{bmatrix}, \tag{4.35}$$

$$\begin{bmatrix} \boldsymbol{\theta}(t+\Delta t) \\ \boldsymbol{\Delta}(t+\Delta t) \end{bmatrix} = \begin{bmatrix} \boldsymbol{\theta}(t) \\ \boldsymbol{\Delta}(t) \end{bmatrix} + \Delta t \begin{bmatrix} \boldsymbol{v}_\theta\left(t+\frac{\Delta t}{2}\right) \\ \boldsymbol{v}_\Delta\left(t+\frac{\Delta t}{2}\right) \end{bmatrix}. \tag{4.36}$$

Here $A_i = -\sum_{j\in\mathcal{N}_i}(I^s_{ij}+I^n_{ij})$ and $\boldsymbol{B} = L^2\bar{\boldsymbol{J}}^{\text{ext}} - \sum_{\langle ij\rangle}(I^s_{ij}+I^n_{ij})\boldsymbol{r}_{ji}$, and the constants $a = 2Q^2+\Delta t$, $b = -2Q^2+\Delta t$, and $d = 2Q^2\Delta t$. In every time step this system of $(N+1)$ coupled equations must be solved, making the RCSJ dynamics far more numerically intensive than Langevin dynamics. Note here that setting $\Delta t = 2Q^2$ makes the constant b in Eq. (4.35) zero, resulting in fully overdamped RSJ dynamics. The leap frog discretized RCSJ equations of motion are then automatically transformed into the RSJ equations of motion, discretized using a forward Euler scheme. Conversely, one could say that RSJ dynamics, integrated using an Euler method with a finite time step, is not fully overdamped, but corresponds to RCSJ dynamics with a damping factor of $Q^2 = \Delta t/2$.

The coefficient matrix in Eq. (4.35) is given by the lattice geometry of the system and is constant throughout the simulation. At first glance, it is tempting to just invert this matrix and use the inverse to multiply the right-hand side in the update scheme above [107, 108]. This is however not a very good idea, since the discrete Laplacian matrix, which makes up essentially the entire coefficient matrix, is *sparse* while its inverse is typically *dense*, see Fig. 4.3. Using the inverse coefficient matrix in the update will make the problem scale poorly as $\mathcal{O}(N^2)$, the computation complexity of a dense matrix-vector multiplication operation. This complexity can be reduced significantly to $\mathcal{O}(N\ln N)$ by employing some fast Fourier transform methods [109, 110]. In our simulations we opt to take advantage of the sparsity of the coefficient matrix and simply solve the system of equations as they stand. With the help of a parallel sparse matrix solver, this approach scales linearly with the number of lattice points N in the system.

4.5 Monte Carlo methods

What we have done so far is to update the system according to some rule based on a stochastic differential equation, derived from more or less physical considerations. By discretizing time, a new configuration of the system has been generated from the previous one in a stepwise manner. This process of generating new states in a random manner, considering only the system at present time is called a *Markov chain*. However, as long as the detailed balance condition of Eq. (4.3) is fulfilled, ensuring the relaxation towards the equilibrium distribution, there is nothing preventing us from constructing

more exotic update schemes based on the Markov chain principle, even ones lacking in physical justification.

Many so called Markov chain Monte Carlo (MC) methods [93, 97, 111] take this approach. These are generally used to effectively sample *equilibrium* distributions. For further discussion it is convenient to break the transition probabilities in Eq. (4.3) into two parts

$$P(i \to j) = t(i \to j)a(i \to j), \tag{4.37}$$

where $t(i \to j)$ is the selection probability, the conditional probability of attempting a move from i to j, given the current state is i, and $a(i \to j)$ is the probability of accepting that move. Usually one takes the selection probabilities to be uniformly distributed and symmetric $t(i \to j) = t(j \to i)$, making their ratios cancel in the detailed balance condition. The acceptance probabilities can now be chosen in any way that ensures detailed balance [Eq. (4.3)], for instance as in Eq. (4.9), where $P(i \to j) \sim e^{-\frac{1}{2}\beta(E_j - E_i)}$. There are of course an infinite number of possible choices to make here, but the optimal one, in the sense that it maximizes the acceptance ratio and therefore produces the most effective algorithm [93], was proposed by Metropolis *et al.* [112] already in 1953. In the *Metropolis choice* we have

$$a(i \to j) = \min\left(e^{-\beta(E_j - E_i)}, 1\right), \tag{4.38}$$

so that updates which lower the energy, $E_j - E_i < 0$, are always accepted, while other moves are accepted with the probability $e^{-\beta(E_j - E_i)}$.

As an example, let us again consider an XY model with N phase variables. In this case, the simplest possible Metropolis MC method is to pick a random phase (i.e., setting the selection probability to $1/N$), and then accept a random rotation of this phase according to Eq. (4.38). Owing to the Metropolis choice, this type of algorithm is more effective in relaxing the system to equilibrium than Langevin or RCSJ dynamics. The important downside, however, is that the time evolution of such an MC algorithm is hard to motivate from a physical perspective, and so care should be taken when interpreting dynamical data.

Close a continuous phase transition the divergence of the correlation length and time makes the dynamics very slow. This is known as *critical slowing down*, and totally destroys the performance of any local update MC scheme, as the one described above. The only way to remedy this is to consider MC moves that change the system on a global scale, so called *cluster algorithms*. The selection and acceptance probabilities will for these algorithms be naturally more complicated than the simple Metropolis choice. For spin models, the two most prominent cluster algorithms are due to Swendsen and Wang [113] and Wolff [114]. Both of these consists of moves that update entire clusters of phase variables, instead of just single phases. The *Wolff algorithm* is by far the easiest to implement on a computer, and is also the most effective one, since it is designed to always flip a cluster in every update step. In Paper 3 we need well converged data for the resistivity at the critical temperature, and therefore found it convenient to employ

the Wolff algorithm in the warmup phase in order to speed up convergence towards equilibrium. This significantly reduced the CPU time spent on equilibration, as well as giving smaller statistical errors in the sampled data. One should remember that the Wolff algorithm only works in zero magnetic field though.

Grand canonical Monte Carlo

The foregoing discussion of Monte Carlo methods assumed a description in terms of the Gibbs or canonical ensemble, where the number of particles is fixed. Considering a system with a fluctuating particle number, described by the grand canonical ensemble, MC moves which create and destroy particles are required. As we will see, the acceptance probabilities of such moves are not equal to the standard $e^{-\beta\Delta E}$, but also depend in some way on the particle number. This makes a *grand canonical Monte Carlo* algorithm [97] considerably more involved to implement than a canonical one. A grand canonical MC scheme is employed in Paper 4 to simulate quantum phase slips in an ultrathin superconducting wire at $T = 0$. This problem is mapped to a gas of interacting vortices (with charge + 1) and antivortices (with charge -1), living in a (1 + 1)D space-time system. For the sake of generality we here consider a two-dimensional classical system at nonzero temperatures. The description is, however, completely analogous to the method used in Paper 4, and by substituting βH for S (the effective action) and $\beta\mu$ for μ, the quantum case at $T = 0$ is recovered.

Generally, the grand canonical configurational partition function for a system of N^+ positively charged and N^- negatively charged particles can be written as

$$Z = \sum_{N^+,N^-} \frac{1}{N^+!N^-!} \prod_{i=1}^{N} \int \frac{d^2 r_i}{\zeta^2} e^{-\beta(H-\mu(N^+ + N^-))}, \tag{4.39}$$

where $N = N^+ + N^-$ is the total number of particles, μ the chemical potential, and ζ the phase space lattice constant. From this one can conclude that the probability for a configuration i with energy E_i, N_i^+ positive particles, and N_i^- negative particles is

$$p_i = \frac{1}{Z} e^{-\beta E_i + \beta\mu(N_i^+ + N_i^-)}. \tag{4.40}$$

The detailed balance condition in Eq. (4.3) now tells us to choose the acceptance probabilities of a move from state i to state j according to

$$\frac{a(i \to j)}{a(j \to i)} = \frac{t(j \to i)}{t(i \to j)} e^{-\beta\Delta E + \beta\mu(\Delta N^+ + \Delta N^-)}, \tag{4.41}$$

with $\Delta E = E_j - E_i$ and $\Delta N^{+/-} = N_j^{+/-} - N_i^{+/-}$. This provides the basis for further discussion of the MC moves.

The MC algorithm used in Paper 4 (originally described in [115] and [116]) consists of essentially five different updates. The simplest move, where a random particle is displaced a random distance, is unproblematic since $\Delta N = 0$, and thus accepted with the

usual Metropolis probability $\min(e^{-\beta\Delta E}, 1)$. The others include creation or destruction of a single particle, or creation or destruction of a neutral pair of particles. The pair move is employed in order to speed up convergence in the superconducting phase, where vortices and antivortices form tightly bound pairs. We consider first the creation of a single particle, $\Delta N^{+/-} = N_j^{+/-} - N_i^{+/-} = 1$. Here, the probability of selecting a specific creation move is just the inverse of the number of places to put a particle, i.e., we have $t(i \to j) = (V/\zeta^2)^{-1}$ in a system of volume V. In the opposite move, the selection probability is just the inverse of the number of ways to pick a particle to destroy, $t(j \to i) = (N_i^{+/-} + 1)^{-1} = (N_j^{+/-})^{-1}$. From Eq. (4.41) we get

$$\frac{a_{ij}}{a_{ji}} = \frac{V}{N_j^{+/-}} e^{-\beta\Delta E + \beta\mu - 2\ln\zeta}. \tag{4.42}$$

Note that the phase space lattice constant ζ only enters here as an unimportant shift of the chemical potential, and can therefore be set to equal to 1. In the move creating a neutral pair of particles ($\Delta N^+ = 1$ and $\Delta N^- = 1$), the selection probability is the combined probability of placing the first particle somewhere in the system and then placing a second particle within a distance d from the first one (d can be varied to optimize convergence). This implies $t(i \to j) = (V\Omega)^{-1}$, where Ω is the area available to create the second particle in. We here set $\Omega = \pi d^2$, corresponding to fully overlapping softcore particles or point particles. When destroying such a pair, we first choose a particle randomly with probability $1/N_j^{+/-}$ and then count the number of particles of opposite charge within a distance d from the first one. Calling this number $N_\Omega^{+/-}$, we get $t(j \to i) = (N_j^{+/-} N_\Omega^{+/-})^{-1}$ and subsequently

$$\frac{a(i \to j)}{a(j \to i)} = \frac{V\Omega}{N_j^{+/-} N_\Omega^{+/-}} e^{-\beta\Delta E + 2\beta\mu}. \tag{4.43}$$

The derived acceptance ratios, given by either Eq. (4.42) or Eq. (4.43), are finally used to construct the acceptance probabilities for creation moves according to the Metropolis choice, $\min(a_{ij}/a_{ji}, 1)$. For destruction moves we take similarly $\min(a_{ji}/a_{ij}, 1)$.

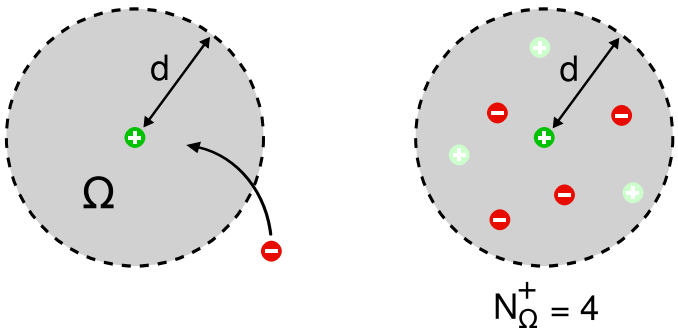

Figure 4.4: Monte Carlo moves that create (left) or destroy (right) a neutral particle pair. Left: The volume to place a second particle in is $\Omega = \pi d^2$ (no volume exclusion). Right: Here the number of negatively charged particles in the volume Ω surrounding the positive particle is $N_\Omega^+ = 4$.

Chapter 5

Summary of papers

The aim of this concluding chapter is to give a more focused introduction to the appended papers, and to summarize and discuss the results.

Paper 1

This work is inspired by the recent experimental discovery of a very large Nernst effect in the pseudogap regime of cuprate high-T_c superconductors [37, 38]. The Nernst effect is usually very small in the normal phase of ordinary metals and therefore offers a sensitive probe to superconducting fluctuation effects in these materials. In large parts of the pseudogap region vortices are highly mobile and form a liquid, and for this reason one possible source of the large Nernst signal might be vortex motion, as argued in a number of papers [37, 38, 39, 40]. Other theoretical papers [41, 117] as well as simulations [118] show that a sizeable Nernst effect can also be obtained by considering Gaussian fluctuations in the amplitude of the superconducting order parameter.

We focus only on the vortex Nernst effect, which we simulate using the simplest possible phase-only model describing a two-dimensional granular superconductor or Josephson junction array in a magnetic field. We study this model using either Langevin or RSJ dynamics. We compute the Nernst signal $e_N = E_y/(-\nabla_x T)$ via a Kubo formula [119, 120], in which the cross-correlation between the transverse electric field E_y and the heat current density in the x direction J_x^Q is integrated over time. By employing periodic boundary conditions combined with a phase twist per unit length Δ across the system as an added degree of freedom (so called fluctuating twist boundary conditions [100]) we can measure $E_y \sim \dot{\Delta}$ at the same time as reducing finite size effects.

We show how the Nernst effect depends strongly on the granular structure and applied magnetic field. The main result is an anomalous behavior of the Nernst signal close to some special magnetic fields. There e_N goes negative, which corresponds to vortex motion from colder to hotter, and therefore heat flow in the direction opposite to the vortex motion. This strange effect is seen in perfectly ordered square and triangular ar-

rays, as well as in moderately disordered systems. We interpret this sign reversal as due to mobile defects in an otherwise pinned the vortex lattice, similar to the observations made in [121]. Given the fact that the anomalous sign of e_N appears also in quite disordered systems, we believe that the effect should be possible to detect in experiments on real Josephson junction arrays or granular superconducting films.

Paper 2

The paper is an extension of Paper 1. We here explore the Nernst signal e_N, the heat conductivity κ, and the electrical resistivity ρ, for the same model as in Paper 1, but now with Langevin, RSJ, and RCSJ dynamics. A key point in this work is the derivation of the heat current, which is needed in the calculation of e_N and κ. The literature contains many derivations of the heat current in superconductors [122, 123, 124, 125]. Over the years, the main issue has been to find the correct form of the heat current in presence of a magnetic field. In this situation any derivation become quite subtle, since magnetization currents must be added to the total charge and transport currents. Although many recent studies [41, 118, 39, 101] seem to employ the form derived in [125], there also exist recent rival suggestions, e.g. [126].

Our approach here is to derive explicit expressions for the heat current within the framework of our models, instead of relying exclusively on previous derivations. We do this in two different ways. First, we write down continuity equations for the local energy of each site on our general discrete lattice, from which the electric contribution to the heat current can be identified. In a similar manner, the magnetization part of the heat current is found by considering a continuity equation for the magnetization energy density defined on the lattice *dual* to the original one.

In the second derivation we use a functional integral representation of the stochastic differential equations defining the Langevin and RCSJ dynamics. This enables us to derive the Kubo formula that we use to calculate e_N. However, since we already know that the general form must be a cross-correlation between the electric field E_y and the heat current density J_x^Q, the obtained expression can also be used to identify the heat current.

The two complementary approaches are applied to both Langevin and RCSJ dynamics, and the respective heat current expressions are found to be on the same form, except for one detail: In the RCSJ case, the *full* current enters into the heat current expression, while for Langevin dynamics it is only the supercurrent. Both expressions agree with the microscopically derived form in [125]. The expressions are thoroughly tested through simulations, where we calculate e_N and κ in two independent ways, either by directly measuring the response to a small temperature gradient $\nabla_x T$, or by using a Kubo formula, and then checking that these results coincide. In the case of the Nernst signal e_N, we use yet a third approach, namely to apply a small electric current J_y and measure the heat current response J_x^Q, and then relate this to e_N via an Onsager relation [127, 128, 30]. An interesting technical detail here, is that to get the same results from all three approaches, we find it necessary to use a fully symmetric

time discretization of the heat current expression. In the RCSJ case this is automatically achieved (by using the symmetric leap frog scheme), while for Langevin dynamics one must symmetrize the discretized form of the heat current. In a spin-wave approximation we analytically show that the harmonic contribution to the thermal conductivity κ in this model diverges in the limit of a small shunting capacitance $C \to 0$. There is also an additional logarithmic system size dependence, which however can be removed by adding a finite onsite capacitance C_0.

We further present e_N, κ and ρ as functions of temperature (for low magnetic fields), and also as a function of the magnetic field for different temperatures. When the magnetic field is varied the behavior is especially dramatic, as geometric frustration greatly impacts these quantities, a well known experimental fact for the electrical resistivity [56], but to our knowledge a new result for the Nernst signal and the heat conductivity. Furthermore, the combined analysis of e_N, κ and ρ provides interesting insights into the transport properties of these granular superconducting systems.

Paper 3

This paper concerns scaling properties of the resistivity and current-voltage (IV) characteristics in two-dimensional superfluids and superconductors at the Berezinskii-Kosterlitz-Thouless (BKT) transition, which is driven by thermal unbinding of vortex-antivortex pairs. One special feature of this transition is the nonlinear IV characteristics $E \sim J^{a(T)}$, at criticality and in the ordered phase, with a temperature dependent exponent $a(T)$. There exist mainly two contesting predictions for the temperature dependence of a, the AHNS theory [129, 130, 131] and that of MWJO [132]. In this work we study this issue by integrating the BKT renormalization group equations up to a length scale (set either by the finite system size, the applied magnetic field or the applied current) where the result can be matched to simple analytical expressions. We show how the two contesting predictions of $a(T)$ can be reconciled. In the limit of large systems the IV exponent agrees with the AHNS result, while for periodic boundary conditions the finite size scaling properties of the system are those predicted by MWJO (if the dynamic critical exponent z is assumed to be 2). We however also allow for $z \neq 2$.

An important point in this analysis is the fact that the vortex fugacity y turns out to be *dangerously irrelevant* for the free vortex density, which is assumed proportional to the resistivity ρ. This means that although y flows to zero at and below T_c, it still affects the scaling of ρ. The scaling is also sensitive to whether a magnetic field is present or not. In zero magnetic field close to T_c, ρ has a strong *multiplicative* logarithmic correction, while it scales as a pure power-law in an asymptotically vanishing field. This has not been taken into account in previous simulation scaling studies, and should also be of significance when interpreting experimental data.

These scaling properties are confirmed in simulations with Langevin and overdamped RCSJ dynamics of the same model used in Paper 1 and 2. By exploiting the pure power-law scaling of the resistivity in an asymptotically vanishing magnetic field, the dynamic critical exponent z is accurately estimated. We find that $z \neq 2$ and is different for

Langevin and RCSJ dynamics, indicating that these two dynamics belong to different dynamic universality classes [82].

Paper 4

Recent experimental evidence [66, 67, 68, 64] holds quantum-fluctuation induced phase slips (QPS) responsible for the breakdown of superconductivity in ultrathin wires.

Starting from an effective microscopic action describing the quantum mechanics of a one-dimensional superconducting wire [72, 73, 74], we reformulate the action and thereby map the problem to a gas of interacting instantons in $(1+1)$D. These instantons appear as vortex configurations in the phase of the superconducting order parameter. The problem is similar to the 2D Coulomb gas, but the interaction between instantons is somewhat modified by the coupling to the electric field in the microscopic effective action. This coupling introduces a screening length λ for the Cooper pairs. At distances much longer than λ (and in very large systems) the instanton interaction reduces to the ordinary logarithmic 2D Coulomb potential, but differs for shorter distances.

Further, a method for obtaining the amplitude of QPS in computer simulations is proposed. This amplitude is also calculated using grand canonical Monte Carlo methods, in which the number of instantons in the system is allowed to fluctuate. We compare these simulation results to a phase diagram suggested in previous experimental [68] studies on ultrathin ($\sim$ 10 nm) MoGe wires. Our simulations seem to reproduce the phase boundaries observed in both long and short wires.

We also calculate the voltage-charge relation, dual to the Josephson current-phase relation in ordinary superconductors. This evolves from a sinusoidal form in the regime of dilute QPS to a sawtooth shape, typically seen in the Coulomb blockade regime, for higher densities. Other, even more exotic, shapes are also observed in system of sizes much larger than the charge screening length λ.

Bibliography

[1] Andreas Andersson and Jack Lidmar. Anomalous Nernst effect and heat transport by vortex vacancies in granular superconductors. *Phys. Rev. B*, 81:060508, 2010.

[2] Andreas Andersson and Jack Lidmar. Influence of vortices and phase fluctuations on thermoelectric transport properties of superconductors in a magnetic field. *Phys. Rev. B*, 83:174502, 2011.

[3] Andreas Andersson and Jack Lidmar. Scaling, finite size effects, and crossovers of the resistivity and current-voltage characteristics in two-dimensional superconductors. *Preprint, arXiv:1203.5317*, 2012.

[4] Andreas Andersson and Jack Lidmar. Modeling and simulations of quantum phase slips in ultrathin superconducting wires. *Manuscript*, 2012.

[5] H. K. Onnes. The resistance of pure mercury at helium temperatures. *Commun. Phys. Lab. Univ. Leiden*, 12:120, 1911.

[6] Dirk van Delft and Peter Kes. The discovery of superconductivity. *Physics Today*, 63(9):38–43, 2010.

[7] M. Tinkham. *Introduction to superconductivity*. Dover Publications, 2004.

[8] J. Bardeen, L. N. Cooper, and J. R. Schrieffer. Theory of Superconductivity. *Phys. Rev.*, 108(5):1175–1204, 1957.

[9] J. G. Bednorz and K. A. Müller. Possible high-T_c superconductivity in the Ba-La-Cu-O system. *Zeitschrift für Physik B Condensed Matter*, 64:189–193, 1986.

[10] J.F. Maguire and J. Yuan. Status of high temperature superconductor cable and fault current limiter projects at American Superconductor. *Physica C: Superconductivity*, 469(15-20):874 – 880, 2009.

[11] RWE Deutschland, Nexans and KIT launch "AmpaCity" project: the world's longest superconductor system to replace inner-city high-voltage cable. *Press release*, 2012.

[12] Yuriy Makhlin, Gerd Schön, and Alexander Shnirman. Quantum-state engineering with Josephson-junction devices. *Rev. Mod. Phys.*, 73:357–400, 2001.

[13] John M. Martinis and Kevin Osborne. Superconducting Qubits and the Physics of Josephson Junctions. *arXiv:cond-mat/0402415v1*, 2004.

[14] V. L. Ginzburg and L. D. Landau. *Zh. Eksp. Teor. Fiz.*, 20(1064), 1950.

[15] A. J. Leggett. *Quantum Liquids: Bose Condensation and Cooper Pairing in Condensensed-Matter Systems*. Oxford University Press, Oxford, 2006.

[16] A. A. Gor'kov. *Zh. Eksp. Teor. Fiz.*, 36(1918), 1959.

[17] W. Meissner and R. Ochsenfeld. Ein neuer Effekt bei Eintritt der Supraleitfähigkeit. *Naturwissenschaften*, 21:787–788, 1933.

[18] L.V. Shubnikov, V.I. Khotkevich, Yu.D. Shepelev, , and Yu.N. Riabinin. *Zh. Eksp. Teor. Fiz.*, 7(221), 1937.

[19] F. London. On the Problem of the Molecular Theory of Superconductivity. *Phys. Rev.*, 74:562–573, 1948.

[20] A. A. Abrikosov. Nobel Lecture: Type-II superconductors and the vortex lattice. *Rev. Mod. Phys.*, 76:975–979, 2004.

[21] A. A. Abrikosov. *Zh. Eksp. Teor. Fiz.*, 32(1442), 1957.

[22] W. H. Kleiner, L. M. Roth, and S. H. Autler. Bulk Solution of Ginzburg-Landau Equations for Type II Superconductors: Upper Critical Field Region. *Phys. Rev.*, 133(5A):A1226–A1227, 1964.

[23] G. Blatter and V. B. Geshkenbein. Vortex Matter. In K. H. Bennemann and John B. Ketterson, editors, *Superconductivity*, pages 495–637. Springer Berlin Heidelberg, 2008.

[24] Daniel S. Fisher, Matthew P. A. Fisher, and David A. Huse. Thermal fluctuations, quenched disorder, phase transitions, and transport in type-II superconductors. *Phys. Rev. B*, 43(1):130–159, 1991.

[25] John Bardeen and M. J. Stephen. Theory of the Motion of Vortices in Superconductors. *Phys. Rev.*, 140:A1197–A1207, 1965.

[26] B. D. Josephson. Potential differences in the mixed state of type II superconductors. *Physics Letters*, 16(3):242 – 243, 1965.

[27] P. W. Anderson and Y. B. Kim. Hard Superconductivity: Theory of the Motion of Abrikosov Flux Lines. *Rev. Mod. Phys.*, 36:39–43, 1964.

[28] Matthew P. A. Fisher. Vortex-glass superconductivity: A possible new phase in bulk high-T_c oxides. *Phys. Rev. Lett.*, 62:1415–1418, 1989.

[29] M. V. Feigel'man, V. B. Geshkenbein, A. I. Larkin, and V. M. Vinokur. Theory of collective flux creep. *Phys. Rev. Lett.*, 63:2303–2306, 1989.

[30] Herbert B. Callen. The Application of Onsager's Reciprocal Relations to Thermoelectric, Thermomagnetic, and Galvanomagnetic Effects. *Phys. Rev.*, 73(11):1349–1358, 1948.

[31] P. R. Solomon and F. A. Otter. Thermomagnetic Effects in Superconductors. *Phys. Rev.*, 164(2):608–618, 1967.

[32] R. P. Huebener and A. Seher. Nernst Effect and Flux Flow in Superconductors. I. Niobium. *Phys. Rev.*, 181(2):701–709, 1969.

[33] T. T. M. Palstra, B. Batlogg, L. F. Schneemeyer, and J. V. Waszczak. Transport entropy of vortex motion in $YBa_2Cu_3O_7$. *Phys. Rev. Lett.*, 64(25):3090–3093, 1990.

[34] S. J. Hagen, C. J. Lobb, R. L. Greene, M. G. Forrester, and J. Talvacchio. Flux-flow Nernst effect in epitaxial $YBa_2Cu_3O_7$. *Phys. Rev. B*, 42(10):6777–6780, 1990.

[35] H.-C. Ri, R. Gross, F. Gollnik, A. Beck, R. P. Huebener, P. Wagner, and H. Adrian. Nernst, Seebeck, and Hall effects in the mixed state of $YBa_2Cu_3O_{7-\delta}$ and $Bi_2Sr_2CaCu_2O_{8+x}$ thin films: A comparative study. *Phys. Rev. B*, 50(5):3312–3329, 1994.

[36] A. V. Ettingshausen and W. H. Nernst. *Wied. Ann.*, 29:343, 1886.

[37] Z. A. Xu, N. P. Ong, Y. Wang, T. Kakeshita, and S. Uchida. Vortex-like excitations and the onset of superconducting phase fluctuation in underdoped $La_{2-x}Sr_xCuO_4$. *Nature*, 406:486–488, 2000.

[38] Yayu Wang, Lu Li, and N. P. Ong. Nernst effect in high-T_c superconductors. *Phys. Rev. B (Condensed Matter and Materials Physics)*, 73(2):024510, 2006.

[39] Daniel Podolsky, Srinivas Raghu, and Ashvin Vishwanath. Nernst Effect and Diamagnetism in Phase Fluctuating Superconductors. *Phys. Rev. Lett.*, 99(11):117004, 2007.

[40] Lu Li, Yayu Wang, Seiki Komiya, Shimpei Ono, Yoichi Ando, G. D. Gu, and N. P. Ong. Diamagnetism and Cooper pairing above T_c in cuprates. *Phys. Rev. B*, 81(5):054510, 2010.

[41] Iddo Ussishkin, S. L. Sondhi, and David A. Huse. Gaussian Superconducting Fluctuations, Thermal Transport, and the Nernst Effect. *Phys. Rev. Lett.*, 89(28):287001, 2002.

[42] Sean A. Hartnoll, Pavel K. Kovtun, Markus Müller, and Subir Sachdev. Theory of the Nernst effect near quantum phase transitions in condensed matter and in dyonic black holes. *Phys. Rev. B*, 76(14):144502, 2007.

[43] Andreas Hackl, Matthias Vojta, and Subir Sachdev. Quasiparticle Nernst effect in stripe-ordered cuprates. *Phys. Rev. B*, 81(4):045102, 2010.

[44] V. J. Emery and S. A. Kivelson. Importance of phase fluctuations in superconductors with small superfluid density. *Nature*, 374(6521):434–437, 1995.

[45] B. D. Josephson. Possible new effects in superconductive tunnelling. *Phys. Lett.*, 1(7):251 – 253, 1962.

[46] V.L. Berezinkii. Destruction of Long-range Order in One-dimensional and Two-dimensional Systems having a Continuous Symmetry Group I. Classical Systems. *Sov. Phys. JETP*, 32:493–500, 1971.

[47] J M Kosterlitz and D J Thouless. Ordering, metastability and phase transitions in two-dimensional systems. *Journal of Physics C: Solid State Physics*, 6(7):1181, 1973.

[48] J. W. Kane and L. P. Kadanoff. Long-range order in superfluid helium. *Phys. Rev.*, 155:80–83, 1967.

[49] N. D. Mermin and H. Wagner. Absence of Ferromagnetism or Antiferromagnetism in One- or Two-Dimensional Isotropic Heisenberg Models. *Phys. Rev. Lett.*, 17:1133–1136, 1966.

[50] P. C. Hohenberg. Existence of Long-Range Order in One and Two Dimensions. *Phys. Rev.*, 158:383–386, 1967.

[51] P.M. Chaikin and T.C. Lubensky. *Principles of condensed matter physics*. Cambridge University Press, 2000.

[52] Petter Minnhagen. The two-dimensional Coulomb gas, vortex unbinding, and superfluid-superconducting films. *Rev. Mod. Phys.*, 59:1001–1066, 1987.

[53] K.K. Likharev. *Dynamics of Josephson junctions and circuits*. Gordon and Breach Science Publishers, 1986.

[54] Richard Feynman. *The Feynman Lectures on Physics*, volume 3. Addison-Wesley, 1963.

[55] Vinay Ambegaokar and Alexis Baratoff. Tunneling between superconductors. *Phys. Rev. Lett.*, 11:104–104, 1963.

[56] Rosario Fazio and Herre van der Zant. Quantum phase transitions and vortex dynamics in superconducting networks. *Physics Reports*, 355(4):235 – 334, 2001.

[57] *Physica B: Condensed Matter*, 222(4):253 – 406, 1996. Proceedings of the ICTP Workshop on Josephson Junction Arrays.

[58] R.S. Newrock. *The Two-dimensional Physics of Josephson Junction Arrays*, volume 54 of *Solid State Physics*. Elsevier, 1999.

[59] William A. Little. Decay of persistent currents in small superconductors. *Phys. Rev.*, 156:396–403, 1967.

[60] J. S. Langer and Vinay Ambegaokar. Intrinsic resistive transition in narrow superconducting channels. *Phys. Rev.*, 164:498–510, 1967.

[61] D. E. McCumber and B. I. Halperin. Time scale of intrinsic resistive fluctuations in thin superconducting wires. *Phys. Rev. B*, 1:1054–1070, 1970.

[62] J. E. Lukens, R. J. Warburton, and W. W. Webb. Onset of Quantized Thermal Fluctuations in "One-Dimensional" Superconductors. *Phys. Rev. Lett.*, 25:1180–1184, 1970.

[63] R. S. Newbower, M. R. Beasley, and M. Tinkham. Fluctuation Effects on the Superconducting Transition of Tin Whisker Crystals. *Phys. Rev. B*, 5:864–868, 1972.

[64] O. V. Astafiev, L. B. Ioffe, S. Kafanov, Yu. A. Pashkin, K. Yu. Arutyunov, D. Shahar, O. Cohen, and J. S. Tsai. Coherent quantum phase slip. *Nature*, 484(7394):355–358, 2012.

[65] N. Giordano. Evidence for Macroscopic Quantum Tunneling in One-Dimensional Superconductors. *Phys. Rev. Lett.*, 61:2137–2140, 1988.

[66] A Bezryadin, CN Lau, and M Tinkham. Quantum suppression of superconductivity in ultrathin nanowires. *Nature*, 404(6781):971–4, 2000.

[67] CN Lau, N Markovic, M Bockrath, A Bezryadin, and M Tinkham. Quantum phase slips in superconducting nanowires. *Phys. Rev. Lett.*, 87(21):217003, 2001.

[68] A. T. Bollinger, R. C. Dinsmore, A. Rogachev, and A. Bezryadin. Determination of the superconductor-insulator phase diagram for one-dimensional wires. *Phys. Rev. Lett.*, 101:227003, 2008.

[69] I M Pop, I Protopopov, F Lecocq, Z Peng, B Pannetier, O Buisson, and W Guichard. Measurement of the effect of quantum phase slips in a Josephson junction chain. *Nature Physics*, 6(8):589–592, 2010.

[70] M. Zgirski, K.-P. Riikonen, V. Touboltsev, and K. Yu. Arutyunov. Quantum fluctuations in ultranarrow superconducting aluminum nanowires. *Phys. Rev. B*, 77:054508, 2008.

[71] Konstantin Yu Arutyunov, Terhi T Hongisto, Janne S Lehtinen, Leena I Leino, and Alexander L Vasiliev. Quantum phase slip phenomenon in ultra-narrow superconducting nanorings. *Scientific reports*, 2:293, 2012.

[72] Andrei Zaikin, Dmitrii Golubev, Anne van Otterlo, and Gergely Zimányi. Quantum Phase Slips and Transport in Ultrathin Superconducting Wires. *Phys. Rev. Lett.*, 78(8):1552–1555, 1997.

[73] Dmitri S. Golubev and Andrei D. Zaikin. Quantum tunneling of the order parameter in superconducting nanowires. *Phys. Rev. B*, 64(1):014504, 2001.

[74] K. Arutyunov, D. Golubev, and A. Zaikin. Superconductivity in one dimension. *Physics Reports*, 464(1-2):1–70, 2008.

[75] J. E. Mooij and Yu. V. Nazarov. Superconducting nanowires as quantum phase-slip junctions. *Nature Physics*, 2(3):169–172, 2006.

[76] K. Matveev, a. Larkin, and L. Glazman. Persistent Current in Superconducting Nanorings. *Phys. Rev. Lett.*, 89(9):2–5, 2002.

[77] Leo P. Kadanoff. Scaling Laws for Ising Models Near Tc. *Physics*, 2:263, 1966.

[78] Kenneth G. Wilson. Renormalization Group and Critical Phenomena. I. Renormalization Group and the Kadanoff Scaling Picture. *Phys. Rev. B*, 4:3174–3183, 1971.

[79] Kenneth G. Wilson. The renormalization group: Critical phenomena and the Kondo problem. *Rev. Mod. Phys.*, 47:773–840, 1975.

[80] N. Goldenfeld. *Lectures on phase transitions and the renormalization group*. Frontiers in physics. Addison-Wesley, Advanced Book Program, 1992.

[81] Michel Le Bellac, Fabrice Mortessagne, and G. George Batrouni. *Equilibrium and Non-equilibrium Statistical Thermodynamics*. Cambridge University Press, 2004.

[82] P. C. Hohenberg and B. I. Halperin. Theory of dynamic critical phenomena. *Rev. Mod. Phys.*, 49(3):435–479, 1977.

[83] K. Huang. *Quantum Field Theory: From Operators to Path Integrals*. John Wiley & Sons, 2010.

[84] J M Kosterlitz. The critical properties of the two-dimensional xy model. *Journal of Physics C: Solid State Physics*, 7(6):1046, 1974.

[85] Jorge V. José, Leo P. Kadanoff, Scott Kirkpatrick, and David R. Nelson. Renormalization, vortices, and symmetry-breaking perturbations in the two-dimensional planar model. *Phys. Rev. B*, 16:1217–1241, 1977.

[86] David R. Nelson and J. M. Kosterlitz. Universal Jump in the Superfluid Density of Two-Dimensional Superfluids. *Phys. Rev. Lett.*, 39:1201–1205, 1977.

[87] D. J. Bishop and J. D. Reppy. Study of the superfluid transition in two-dimensional ^{4}He films. *Phys. Rev. Lett.*, 40:1727–1730, 1978.

[88] A. F. Hebard and A. T. Fiory. Evidence for the Kosterlitz-Thouless Transition in Thin Superconducting Aluminum Films. *Phys. Rev. Lett.*, 44:291–294, 1980.

[89] Matthias Vojta. Quantum phase transitions. *Reports on Progress in Physics*, 66(12):2069, 2003.

[90] A. Altland and B.D. Simons. *Condensed matter field theory*. Cambridge University Press, 2010.

[91] S. Sachdev. *Quantum Phase Transitions*. Cambridge University Press, 2011.

[92] S. L. Sondhi, S. M. Girvin, J. P. Carini, and D. Shahar. Continuous quantum phase transitions. *Rev. Mod. Phys.*, 69:315–333, 1997.

[93] M.E.J. Newman and G.T. Barkema. *Monte Carlo methods in statistical physics*. Clarendon Press, 1999.

[94] Hagen Kleinert. *Path Integrals in Quantum Mechanics, Statistics, Polymer Physics, and Financial Markets, 3rd Edition*. World Scientific, 2004.

[95] L. Onsager and S. Machlup. Fluctuations and Irreversible Processes. *Phys. Rev.*, 91:1505–1512, 1953.

[96] P.E. Kloeden and E. Platen. *Numerical solution of stochastic differential equations*. Springer-Verlag, 1992.

[97] D. Frenkel and B. Smit. *Understanding molecular simulation: from algorithms to applications*. Academic Press, 2002.

[98] N.G. van Kampen. *Stochastic processes in physics and chemistry*. Elsevier, 2007.

[99] W. Coffey, Y.P. Kalmykov, and J.T. Waldron. *The Langevin equation: with applications to stochastic problems in physics, chemistry, and electrical engineering*. World Scientific, 2004.

[100] Beom Jun Kim, Petter Minnhagen, and Peter Olsson. Vortex dynamics for two-dimensional XY models. *Phys. Rev. B*, 59(17):11506–11522, 1999.

[101] Anatoly Larkin and Andrei Varlamov. *Theory of Fluctuations in Superconductors*. Oxford University Press, New York, 2009.

[102] J. B. Johnson. Thermal Agitation of Electricity in Conductors. *Phys. Rev.*, 32(1):97, 1928.

[103] H. Nyquist. Thermal Agitation of Electric Charge in Conductors. *Phys. Rev.*, 32(1):110–113, 1928.

[104] W.C. Stewart. Current-voltage characteristics of Josephson junctions. *Applied Physics Letters*, 12(8):277–280, 1968.

[105] McCumber, D.E. Effect of ac impedance on dc voltage-current characteristics of superconductor weak-link junctions. *Journal of Applied Physics*, 39(7):3113–3118, 1968.

[106] J. S. Chung, K. H. Lee, and D. Stroud. Dynamical properties of superconducting arrays. *Phys. Rev. B*, 40(10):6570–6580, 1989.

[107] S R Shenoy. Dynamic conductivity of a two-dimensional Josephson junction array. *Journal of Physics C: Solid State Physics*, 18(26):5163, 1985.

[108] K. K. Mon and S. Teitel. Phase Coherence and Nonequilibrium Behavior in Josephson Junction Arrays. *Phys. Rev. Lett.*, 62(6):673–676, 1989.

[109] H. Eikmans and J. E. van Himbergen. Dynamic simulations of arrays of Josephson junctions. *Phys. Rev. B*, 41(13):8927–8932, 1990.

[110] Verónica I. Marconi and Daniel Domínguez. Melting and transverse depinning of driven vortex lattices in the periodic pinning of Josephson junction arrays. *Phys. Rev. B*, 63(17):174509, 2001.

[111] B.A. Berg. *Markov Chain Monte Carlo Simulations And Their Statistical Analysis: With Web-based Fortran Code*. World Scientific, 2004.

[112] N. Metropolis, A. W. Rosenbluth, M. N. Rosenbluth, A. H. Teller, and E. Teller. Equation of State Calculations by Fast Computing Machines. *J. Chem. Phys.*, 21:1087–1092, 1953.

[113] Robert H. Swendsen and Jian-Sheng Wang. Nonuniversal critical dynamics in Monte Carlo simulations. *Phys. Rev. Lett.*, 58:86–88, 1987.

[114] Ulli Wolff. Collective Monte Carlo Updating for Spin Systems. *Phys. Rev. Lett.*, 62:361–364, 1989.

[115] John P. Valleau and L. Kenneth Cohen. Primitive model electrolytes. I. Grand canonical Monte Carlo computations. *J. Chem. Phys.*, 72(11):5935–5941, 1980.

[116] Jack Lidmar and Mats Wallin. Monte Carlo simulation of a two-dimensional continuum Coulomb gas. *Phys. Rev. B*, 55:522–530, 1997.

[117] M. N. Serbyn and M. A. Skvortsov and A. A. Varlamov and Victor Galitski. Giant nernst effect due to fluctuating cooper pairs in superconductors. *Phys. Rev. Lett.*, 102(6):067001, 2009.

[118] Subroto Mukerjee and David A. Huse. Nernst effect in the vortex-liquid regime of a type-II superconductor. *Phys. Rev. B*, 70(1):014506, 2004.

[119] Ryogo Kubo. Statistical-Mechanical Theory of Irreversible Processes. I. General Theory and Simple Applications to Magnetic and Conduction Problems. *Journal of the Physical Society of Japan*, 12(6):570–586, 1957.

[120] J. M. Luttinger. Theory of Thermal Transport Coefficients. *Phys. Rev.*, 135(6A):A1505–A1514, 1964.

[121] M. Franz and S. Teitel. Vortex-lattice melting in two-dimensional superconducting networks and films. *Phys. Rev. B*, 51(10):6551–6574, 1995.

[122] Albert Schmid. A time dependent Ginzburg-Landau equation and its application to the problem of resistivity in the mixed state. *Zeitschrift für Physik B Condensed Matter*, 5(4):302–317, Oct 1966.

[123] Christiane Caroli and Kazumi Maki. Motion of the Vortex Structure in Type-II Superconductors in High Magnetic Field. *Phys. Rev.*, 164(2):591–607, 1967.

[124] Kazumi Maki. Thermomagnetic Effects in Dirty Type-II Superconductors. *Phys. Rev. Lett.*, 21(26):1755–1757, 1968.

[125] Chia-Ren Hu. Heat-current operator and transport entropy of vortices in type-II superconductors. *Phys. Rev. B*, 13(11):4780–4783, 1976.

[126] A. Sergeev, M. Yu. Reizer, and V. Mitin. Heat current in the magnetic field: Nernst-Ettingshausen effect above the superconducting transition. *Phys. Rev. B*, 77(6):064501, 2008.

[127] Lars Onsager. Reciprocal Relations in Irreversible Processes. I. *Phys. Rev.*, 37(4):405–426, 1931.

[128] Lars Onsager. Reciprocal Relations in Irreversible Processes. II. *Phys. Rev.*, 38(12):2265–2279, 1931.

[129] Vinay Ambegaokar, B. I. Halperin, David R. Nelson, and Eric D. Siggia. Dissipation in Two-Dimensional Superfluids. *Phys. Rev. Lett.*, 40(12):783–786, 1978.

[130] Vinay Ambegaokar, B. I. Halperin, David R. Nelson, and Eric D. Siggia. Dynamics of superfluid films. *Phys. Rev. B*, 21(5):1806–1826, 1980.

[131] B. I. Halperin and David R. Nelson. Resistive transition in superconducting films. *JLTP*, 36:599–616, 1979.

[132] Petter Minnhagen, Olof Westman, Anna Jonsson, and Peter Olsson. New Exponent for the Nonlinear IV Characteristics of a Two Dimensional Superconductor. *Phys. Rev. Lett.*, 74(18):3672–3675, 1995.

Part II

Scientific papers